frontiers in Chemistry

ORIGINAL RESEARCH
published: 18 September 2019
doi: 10.3389/fchem.2019.00597

Novel Tautomerisation Mechanisms of the Biologically Important Conformers of the Reverse Löwdin, Hoogsteen, and Reverse Hoogsteen G* · C* DNA Base Pairs *via* Proton Transfer: A Quantum-Mechanical Survey

Ol'ha O. Brovarets'[1,2†], *Timothy A. Oliynyk*[1†] *and Dmytro M. Hovorun*[1,3,4*†]

[1] *Department of Molecular and Quantum Biophysics, Institute of Molecular Biology and Genetics, National Academy of Sciences of Ukraine, Kyiv, Ukraine,* [2] *Department of Pharmacology, Bohomolets National Medical University, Kyiv, Ukraine,* [3] *Department of Molecular Biotechnology and Bioinformatics, Institute of High Technologies, Taras Shevchenko National University of Kyiv, Kyiv, Ukraine,* [4] *Department of Pathophysiology, Bohomolets National Medical University, Kyiv, Ukraine*

OPEN ACCESS

Edited by:
Yong Wang,
Ningbo University, China

Reviewed by:
Santiago Tolosa Arroyo,
University of Extremadura, Spain
Dingguo Xu,
Sichuan University, China

****Correspondence:***
Dmytro M. Hovorun
d.m.hovorun@imbg.org.ua

†ORCID:
Ol'ha O. Brovarets'
orcid.org/0000-0002-8929-293X
Timothy A. Oliynyk
orcid.org/0000-0002-2276-033X
Dmytro M. Hovorun
orcid.org/0000-0002-5579-5520

Specialty section:
This article was submitted to Theoretical and Computational Chemistry, a section of the journal Frontiers in Chemistry

Received: *05 June 2019*
Accepted: *12 August 2019*
Published: *18 September 2019*

Citation:
Brovarets' OO, Oliynyk TA and Hovorun DM (2019) Novel Tautomerisation Mechanisms of the Biologically Important Conformers of the Reverse Löwdin, Hoogsteen, and Reverse Hoogsteen G · C* DNA Base Pairs via Proton Transfer: A Quantum-Mechanical Survey. Front. Chem. 7:597. doi: 10.3389/fchem.2019.00597*

For the first time, in this study with the use of QM/QTAIM methods we have exhaustively investigated the tautomerization of the biologically-important conformers of the G* · C* DNA base pair—reverse Löwdin G* · C*(rWC), Hoogsteen G*′ · C*(H), and reverse Hoogsteen G*′ · C*(rH) DNA base pairs—*via* the single (SPT) or double (DPT) proton transfer along the neighboring intermolecular H-bonds. These tautomeric reactions finally lead to the formation of the novel G·C^*_{O2}(rWC), G^*_{N2}·C(rWC), $G^{*\prime}_{N2}$·C(rWC), G^*_{N7}·C(H), and $G^{*\prime}_{N7}$·C(rH) DNA base mispairs. Gibbs free energies of activation for these reactions are within the range 3.64–31.65 kcal·mol^{-1} in vacuum under normal conditions. All TSs are planar structures (C_s symmetry) with a single exception—the essentially non-planar transition state $TS_{G^*\cdot C^*(rWC)\leftrightarrow G^+\cdot C^-(rWC)}$ (C_1 symmetry). Analysis of the kinetic parameters of the considered tautomerization reactions indicates that in reality only the reverse Hoogsteen G*′·C*(rH) base pair undergoes tautomerization. However, the population of its tautomerised state $G^{*\prime}_{N7}$·C(rH) amounts to an insignificant value—$2.3\cdot10^{-17}$. So, the G* · C*(rWC), G*′ · C*(H), and G*′ · C*(rH) base pairs possess a permanent tautomeric status, which does not depend on proton mobility along the neighboring H-bonds. The investigated tautomerization processes were analyzed in details by applying the author's unique methodology—sweeps of the main physical and chemical parameters along the intrinsic reaction coordinate (IRC). In general, the obtained data demonstrate the tautomeric mobility and diversity of the G* · C* DNA base pair.

Keywords: single proton transfer, double proton transfer, conformer, reverse Löwdin base pair, Hoogsteen, reverse Hoogsteen, transition state, quantum-mechanical calculation

INTRODUCTION

The study of the tautomerization mechanisms of the hydrogen (H) bonded nucleotide base pair is an important topic of modern quantum biophysics, biochemistry, molecular, and structural biology (Sinden, 1994; Sponer and Lankas, 2006; Alkorta et al., 2018). For over 65 years, this area of research has been under the intense scrutiny of both theoretics and experimentators, since the establishment of the spatial organization of DNA and formulation of the so-called "tautomeric hypothesis of the origin of spontaneous point mutations (transitions and transversions)" (Watson and Crick, 1953a,b; Erdmann et al., 2014) for this biologically important macromolecule—carrier of the genetic information, which is transmitted from generation to generation.

Lately, this tautomeric hypothesis has been experiencing an era of renaissance (Brovarets' and Hovorun, 2018). Thus, for the first time, within the framework of this hypothesis the new structural mechanisms of the tautomerization of pairs of nucleotide bases have been discovered, in which the transition of bases within the base pair into the mutagenic tautomeric form is accompanied by a significant change in the geometry of the base pair itself (Brovarets' and Hovorun, 2009, 2015a,b,c,d,e, 2016, 2018).

However, at the studying of the nature of the mutagenic tautomerization of DNA bases, the researchers limited themselves to the A·T and G·C Watson-Crick base pairs (Löwdin, 1963, 1966; Florian et al., 1994; Gorb et al., 2004; Bertran et al., 2006; Brovarets' and Hovorun, 2014a,b). Now this problem is considered more complex with the involvement of several biologically important conformers of these pairs (Hoogsteen, 1963; Pous et al., 2008; Alvey et al., 2014; Brovarets' and Hovorun, 2014a,b; Nikolova et al., 2014; Acosta-Reyes et al., 2015; Poltev et al., 2016; Zhou, 2016; Szabat and Kierzek, 2017; Ye et al., 2017).

These observations do not only allow to penetrate deeper into the essence of the phenomenon being studied, but also to answer, in particular, on a biologically important question—"Why *Nature* has exactly chosen the Watson-Crick DNA base pairs as elementary structural units for the construction of genetic material?"

Nowadays, there is an explicit bias to the A·T DNA base pair at the investigations of this type. This is due to a large number of circumstances, which will be outlined and discussed below.

Thus, it is widely known that the classical A·T(WC) Watson-Crick DNA base pair (Brovarets' and Hovorun, 2014b) may acquire different biologically significant conformations with various organization of the three intermolecular H-bonds—reverse Watson-Crick A·T(rWC), Hoogsteen A·T(H), and reverse Hoogsteen A·T(rH), which have been comprehensively studied in the literature (Hoogsteen, 1963; Pous et al., 2008; Alvey et al., 2014; Brovarets' and Hovorun, 2014b; Nikolova et al., 2014; Acosta-Reyes et al., 2015; Poltev et al., 2016; Zhou, 2016; Szabat and Kierzek, 2017; Ye et al., 2017).

Thus, in particular, in previous works (Hoogsteen, 1963; Pous et al., 2008; Brovarets' and Hovorun, 2010, 2014b, 2015f; Brovarets', 2013a,b; Alvey et al., 2014; Nikolova et al., 2014; Acosta-Reyes et al., 2015; Poltev et al., 2016; Zhou, 2016; Szabat and Kierzek, 2017; Ye et al., 2017; Brovarets' et al., 2018a,b,c,d,e,f; Brovarets' and Tsiupa, 2019) by the methods of quantum chemistry we have investigated in details the potential (electronic) energy surface of each of the four biologically important A·T DNA base pairs—Watson-Crick A·T(WC), reverse Watson-Crick A·T(rWC), Hoogsteen A·T(H) and reverse Hoogsteen A·T(rH), leading to the novel conformational or tautomeric states of these base pairs. It was theoretically demonstrated that these A·T(WC/rWC/H/rH) base pairs possess unique ability to perform conformationally-tautomeric transition into the planar wobble $A^*{\cdot}T(w)$, $A{\cdot}T^*_{O2}(w)$, and $A{\cdot}T^*(w)$ base mispairs, non-planar wobble $A{\cdot}T(w_{WC})$, $A{\cdot}T(w_{rWC})$, $A{\cdot}T(w_H)$, and $A{\cdot}T(w_{rH})$ base mispairs and incorrect $A{\cdot}T^*(w^{\perp}_{WC})$, $A{\cdot}T^*_{O2}(w^{\perp}_{rWC})$, $A{\cdot}T^*(w^{\perp}_{H})$, and $A{\cdot}T^*_{O2}(w^{\perp}_{rH})$ base mispairs containing mutagenic tautomers of the DNA bases, and also their interconversions between each other through the non-planar transition states *via* the structural or conformational rearrangements and intramolecular proton transfer along the intermolecular H-bonds.

In contrast to this, the classical G·C Watson-Crick DNA base pair (Brovarets', 2013b; Brovarets' and Hovorun, 2014a, 2015f) could not acquire different conformations in the main tautomeric state due to the obstacles presented by its geometrical structure. This, however, can be overcome through the G·C(WC)→G*·C*(WC) tautomerisation *via* the double proton transfer (DPT), according to Löwdin's mechanism (Löwdin, 1963, 1966; Brovarets' and Hovorun, 2014a, 2018). This Löwdin's reaction can proceed over the barrier of tautomerization or under the barrier *via* the tunneling (Parker and Van Everv, 1971; Boutis, 1992; Al-Khalili and McFadden, 2014; Brovarets' and Hovorun, 2015g; Godbeer et al., 2015; Turaeva and Brown-Kennerly, 2015; Meisner and Kastner, 2016; Roßbach and Ochsenfeld, 2017; McFadden and Al-Khalili, 2018; Pusuluk et al., 2018; Smedarchina et al., 2018; Shekaari and Jafari, 2019; Srivastava, 2019).

At this, the so-called Löwdin G* · C*(WC) base pair with geometry close to Watson-Crick, which is created in such a way, involving mutagenic tautomers of the DNA bases, can acquire similarly to the A·T(WC) base pair different conformations (Brovarets' and Hovorun, 2010, 2015f; Brovarets', 2013a,b; Brovarets' et al., 2018a,b,c,d,e,f; Brovarets' and Tsiupa, 2019)—reverse Löwdin G* · C*(rWC), Hoogsteen G*′ · C*(H) and reverse Hoogsteen G*′ · C*(rH) (Brovarets', 2013b) (here and below the superscript "*" denotes the rare tautomeric form of the DNA base (Glushenkov and Hovorun, 2016) and "′"—*trans*-orientation of the OH group). This demonstrates quite unexpected role of the Löwdin's tautomerisation for the conformational variety.

Currently, there is no mention of reverse Löwdin G* · C*(rWC), Hoogsteen G*′ · C*(H) and reverse Hoogsteen G*′ · C*(rH) conformers or their tautomerisation *via* the DPT along the intermolecular H-bonds, despite a great number of investigations devoted to this important phenomenon.

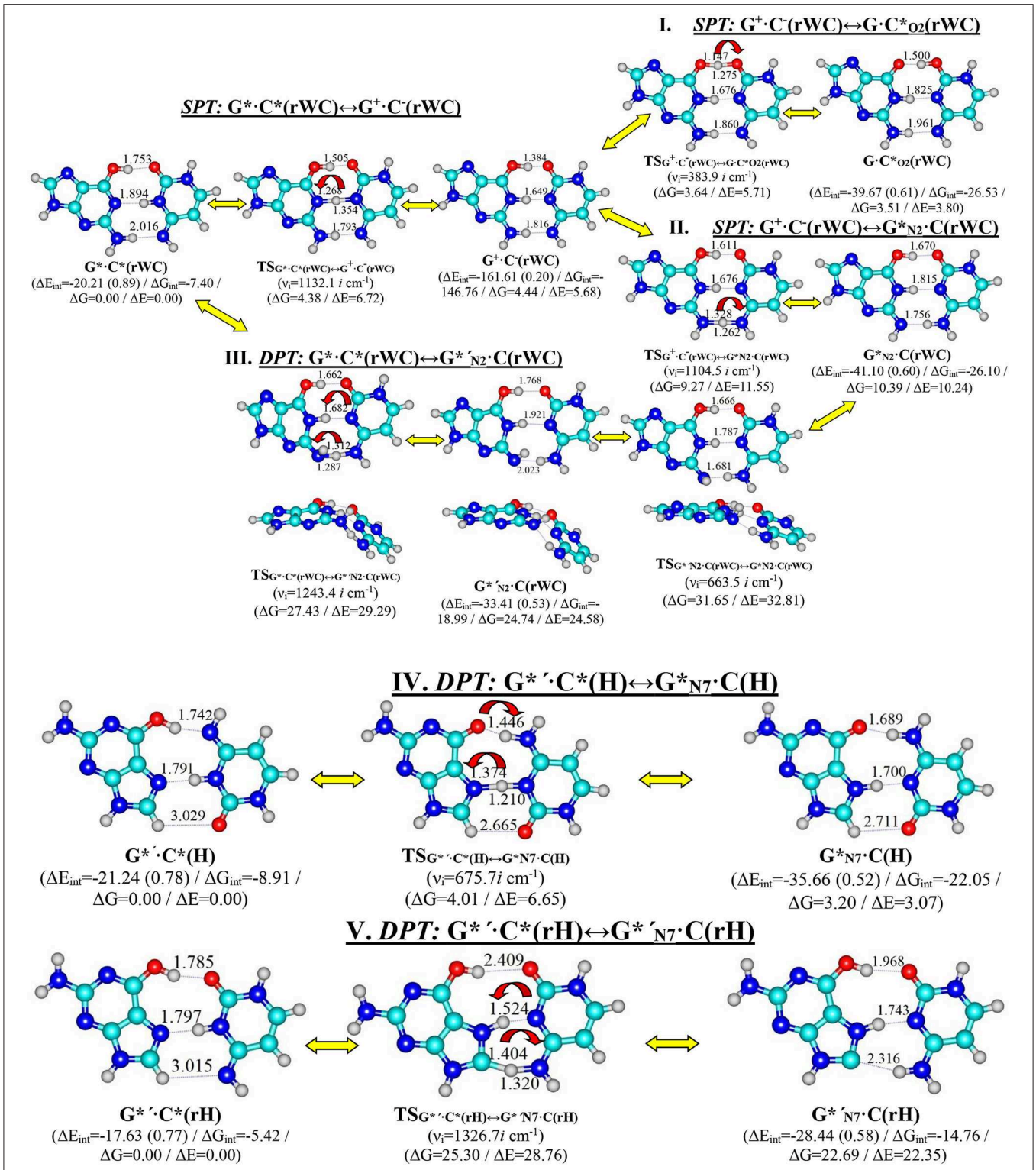

FIGURE 1 | Discovered new reaction pathways of the tautomerization in the reverse Watson-Crick G*·C*(rWC) – I. G*·C*(rWC)↔G^{+}·C^{-}(rWC)↔G·C*$_{O2}$(rWC), II. G*·C*(rWC)↔G^{+}·C^{-}(rWC)↔G*$_{N2}$·C(rWC), III. G*·C*(rWC)↔G*′$_{N2}$·C(rWC), Hoogsteen G*′·C*(H) – IV. G*′·C*(H)↔G*$_{N7}$·C(H)—and reverse Hoogsteen G*′·C*(rH) – V. G*′·C*(rH)↔G*′$_{N7}$·C(rH) – DNA base pairs through the single or double proton transfer. Electronic ΔE_{int} and Gibbs free ΔG_{int} energies of the interaction [MP2/6-311++G(2df,pd)//B3LYP/6-311++G(d,p) level of theory, in kcal·mol^{-1}], relative Gibbs free energies ΔG, and electronic energies ΔE [MP2/aug-cc-pVDZ//B3LYP/6-311++G(d,p) level of theory in the continuum with $\varepsilon = 1$ at T = 298.15 in kcal·mol^{-1}] are presented below complexes in brackets. Dotted lines indicate AH···B H-bonds – their lengths H···B are presented in angstroms; carbon atoms are in light-blue, nitrogen—in dark-blue, hydrogen—in gray and oxygen – in red. ν_i—imaginary frequencies at the TSs of the tautomeric/conformational transitions.

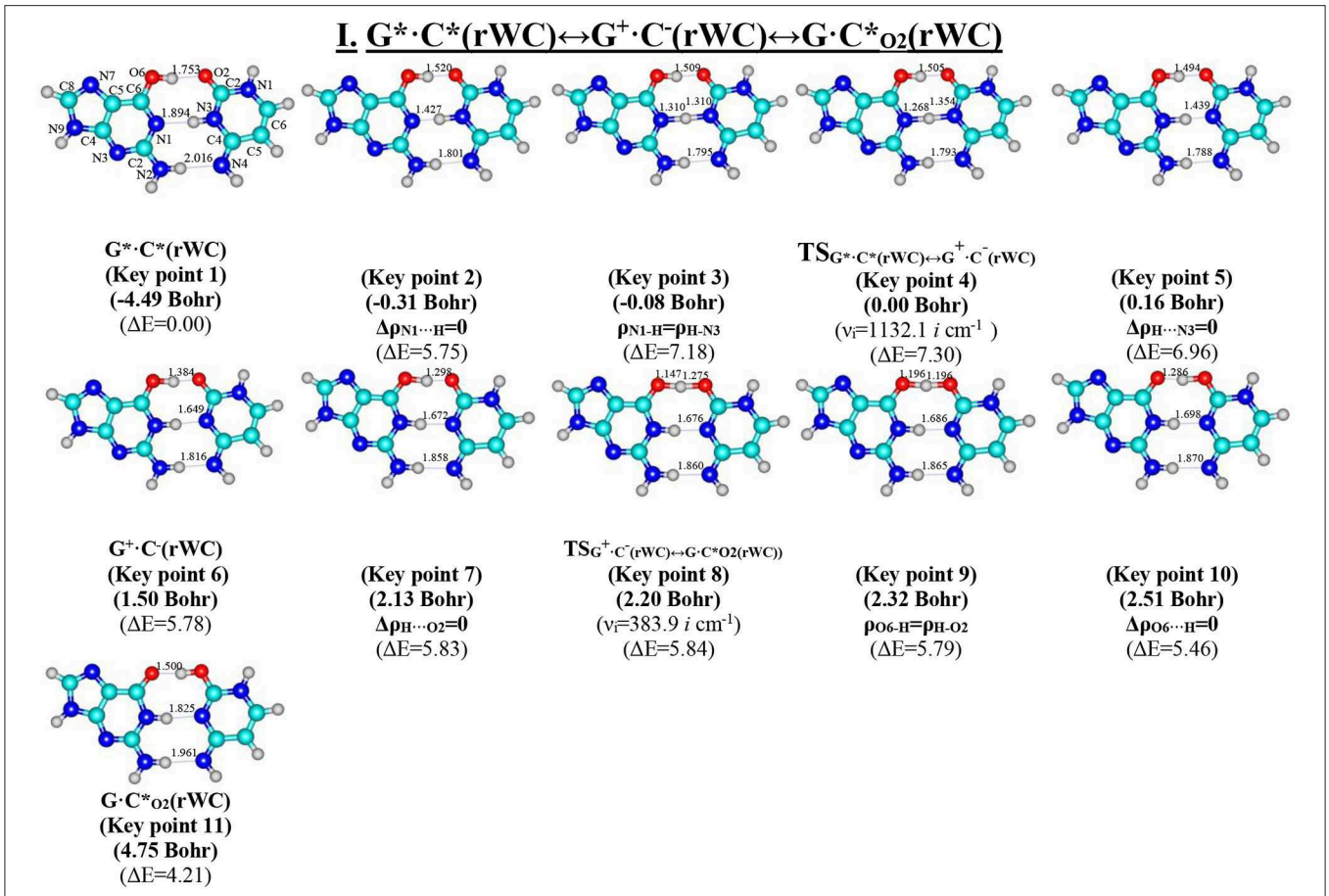

FIGURE 2 | Geometric structures of the 11 key points describing the evolution of the I. G*·C*(rWC)↔G^{+}·C^{-}(rWC)↔G·C^{*}_{O2}(rWC) tautomerisation *via* the sequential SPT along the IRC obtained at the B3LYP/6-311++G(d,p) level of theory *in vacuo*. Coordinates of the 11 key points, their relative electronic energies ΔE (in kcal·mol^{-1} obtained at the B3LYP/6-311++G(d,p) level of theory in vacuum at T = 298.15) and imaginary frequencies ν_i (cm^{-1}) at the TSs of their interconversions are presented below them in brackets (see **Table 3**). For more detailed designations see **Figure 1**.

In our previous studies we have comperehensively investigated the tautomerisation *via* the DPT of the canonical A·T(WC) (Brovarets' and Hovorun, 2014b, 2015g) and G·C(WC) (Brovarets' and Hovorun, 2014a) Watson-Crick DNA base pairs, and also of the incorrect DNA base pairs—wobble G·T base pair (Brovarets' et al., 2015), short C·T (Brovarets' and Hovorun, 2013a), C*·C (Brovarets' and Hovorun, 2013b), T*·T (Brovarets' et al., 2014a), H·C (Brovarets' and Hovorun, 2013c; Brovarets' et al., 2013a) and H* · T (Brovarets' and Hovorun, 2013c; Brovarets' et al., 2013a); long A·A* (Brovarets' and Hovorun, 2013d), A·G (Brovarets' et al., 2014b), G·G* (Brovarets' and Hovorun, 2014c), H·H (Brovarets' and Hovorun, 2013c; Brovarets' et al., 2013a), H* · H (Brovarets' and Hovorun, 2013c; Brovarets' et al., 2013b) and H·A (Brovarets' and Hovorun, 2013c; Brovarets' et al., 2014c); Watson-Crick-like A·C* (Brovarets' and Hovorun, 2015h), G*·T (Brovarets' and Hovorun, 2015i), G·A_{syn} (Brovarets' and Hovorun, 2014d), A*·G^{*}_{syn} (Brovarets' and Hovorun, 2014d), A*·A_{syn} (Brovarets' et al., 2014d), G·G^{*}_{syn} (Brovarets' and Hovorun, 2014e), T·2AP*(w) (Brovarets' et al., 2017; Brovarets' and Hovorun, 2019a), and G·2AP*(w) (Brovarets' et al., 2017; Brovarets' and Hovorun, 2019a) base mispairs and protein-DNA complexes (Brovarets' et al., 2012), which we have summarized in our review (Brovarets' and Hovorun, 2019b), devoted to the microstructural mechanisms of the tautomerization by the proton transfer along the neighboring intermolecular H-bonds in 22 biologically important pairs of nucleotide bases in the framework of the author's method, which enable to trace the evolution of the physico-chemical parameters along the intrinsic reaction coordinate (IRC).

In this study, we aim to reapply the approach, which we launched in our previous works (Brovarets' et al., 2018a,b,c,d,e,f; Brovarets' and Tsiupa, 2019) in order to investigate in details the tautomerisation of the reverse Löwdin G* · C*(rWC), Hoogsteen G*′ · C*(H), and reverse Hoogsteen G*′ · C*(rH) base pairs *via* PT along the neighboring intermolecular H-bonds.

As a result of the previous investigations, it was established that proton mobility along the intermolecular H-bonds does not change the tautomeric status of the investigated base pairs. Along with this biologically important conclusion, for the first time we have obtained a number of important physical and chemical

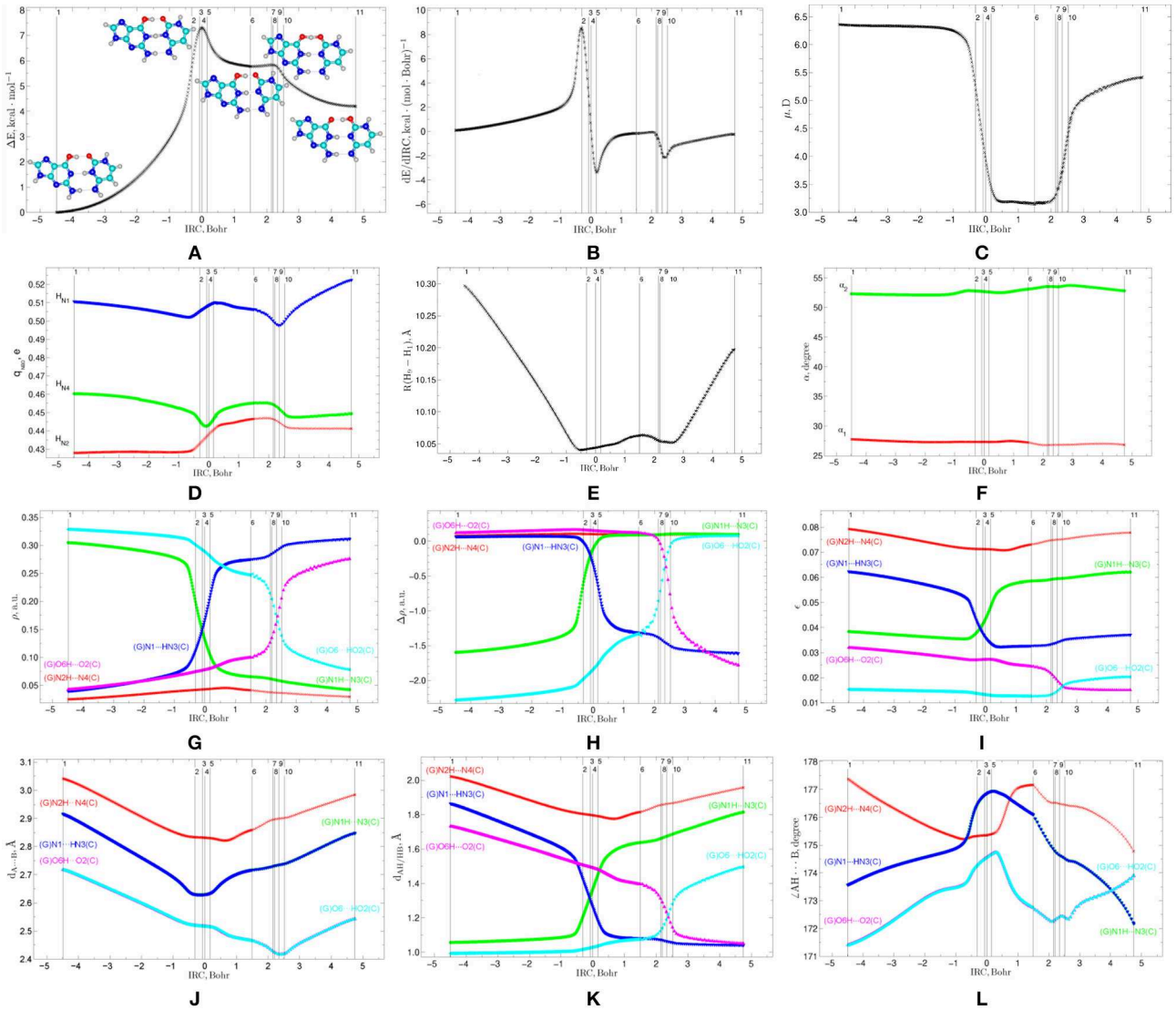

FIGURE 3 | Profiles of: **(A)** the relative electronic energy ΔE, **(B)** the first derivative of the electronic energy with respect to the IRC (dE/dIRC), **(C)** the dipole moment μ, **(D)** the NBO charges q_{NBO}, **(E)** the distance R(H_1-H_9) between the H_1 and H_9 glycosidic hydrogens, **(F)** the α_1 (∠N1H_1(C)H_9(G)) and α_2 (∠N9H_9(G)H_1(C)) glycosidic angles, **(G)** the electron density ρ; **(H)** the Laplacian of the electron density Δρ, **(I)** the ellipticity ε at the (3,−1) BCPs, **(J)** the distance $d_{A...B}$ between the electronegative A and B atoms; **(K)** the distance $d_{AH/HB}$ between the hydrogen and electronegative A or B atoms and **(L)** the angle ∠AH···B of the covalent and hydrogen bonds along the IRC of the investigated I. G*·C*(rWC)↔G^+·C^-(rWC)↔G·C^*_{O2}(rWC) tautomerisation *via* the sequential SPT obtained at the B3LYP/6-311++G(d,p) level of theory in vacuum.

characteristics. As such, it was documented that tautomerisation of the reverse Löwdin G* · C*(rWC) DNA base pair along the middle H-bond induces analogous SPT along its upper and lower H-bonds. Moreover, for the first time we have described the formation of a dynamically stable base pair with participation of the yilidic form of the purine base, formed through asynchronous DPT and participation of the CH group as proton donor.

Digging deeper into the mechanisms of tautomerisation of the reverse Löwdin G* · C*(rWC), Hoogsteen G*′ · C*(H), and reverse Hoogsteen G*′ · C*(rH) base pairs, we have carefully obtained sweeps of the physical and chemical parameters that characterize proton mobility along the IRC. Firstly, we have established a monotonic dependence of the base pair's dipole moment along the IRC. Second, it was shown that the SPT processes are characterized by the presence of 6 key points.

COMPUTATIONAL METHODS

Density Functional Theory Geometry and Vibrational Frequencies Calculations

All calculations of the geometries and harmonic vibrational frequencies of the considered base mispairs and transition states

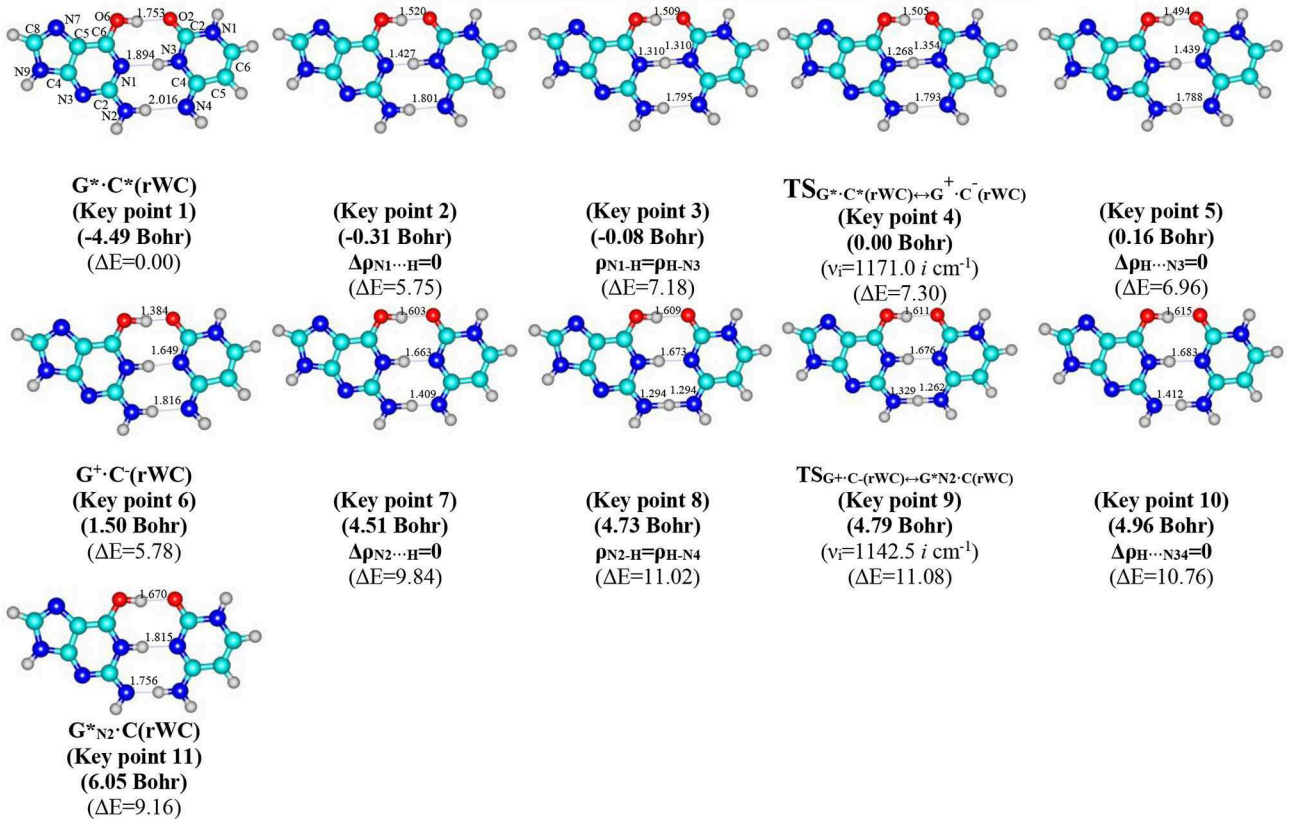

FIGURE 4 | Geometric structures of the 11 key points describing the evolution of the II. G*·C*(rWC)↔G^+·C^-(rWC)↔G^*_{N2}·C(rWC) tautomerisation *via* the sequential SPT along the IRC obtained at the B3LYP/6-311++G(d,p) level of theory *in vacuo* (see **Table 4**). For more detailed designations see **Figure 2**.

of their conversion have been conducted using Gaussian'09 package (Frisch et al., 2010) at the DFT B3LYP/6-311++G(d,p) level of theory (Lee et al., 1988; Parr and Yang, 1989; Tirado-Rives and Jorgensen, 2008), that has been already applied for analogous systems and approved to give accurate geometrical structures, normal mode frequencies, barrier heights, and characteristics of intermolecular H-bonds (Matta, 2010; Arabi and Matta, 2018; Gatti et al., 2018). We have used a scaling factor equal to 0.9668 in order to correct harmonic frequencies for the investigated base pairs (Brovarets' and Hovorun, 2010, 2015f; Brovarets', 2013a,b; Palafox, 2014; El-Sayed et al., 2015; Brovarets' et al., 2018a,b,c,d,e,f; Brovarets' and Tsiupa, 2019). We have associated structures, which were localized on the potential energy landscape by means of Synchronous Transit-guided Quasi-Newton method (Peng et al., 1996), to the minima or transition state (TS) by the absence or presence of the imaginary frequency in the vibrational spectra of the complexes, respectively. We used standard TS theory (Atkins, 1998) in order to estimate the forward and reverse barriers of the investigated tautomerisation reaction.

IRC Calculations

Reaction pathways have been monitored by following IRC in the forward and reverse directions from each TS using Hessian-based predictor-corrector algorithm for integration (Hratchian and Schlegel, 2005). In such a way we ensure that it was received proper reaction pathway from reactants to products. Further, we have obtained the sweeps of the energetic, polar, and geometric characteristics of the H-bonds and base pairs along the IRC by calculating them at each point of the IRC (Brovarets' et al., 2017, 2018g,h).

Single Point Energy Calculations

In order to take into account electronic correlation effects, we followed geometry optimizations with single point energy calculations using MP2 level of theory (Frisch et al., 1990) and 6-311++G(2df,pd) Pople's basis set of valence triple-ζ quality (Hariharan and Pople, 1973; Krishnan et al., 1980) and aug-cc-pVDZ Dunning's cc-type basis set (Kendall et al., 1992), augmented with polarization and/or diffuse function.

The Gibbs free energy G for all structures was calculated by the formula:

$$G = E_{el} + E_{corr}, \quad (1)$$

where E_{el}–electronic energy, while E_{corr}–thermal correction.

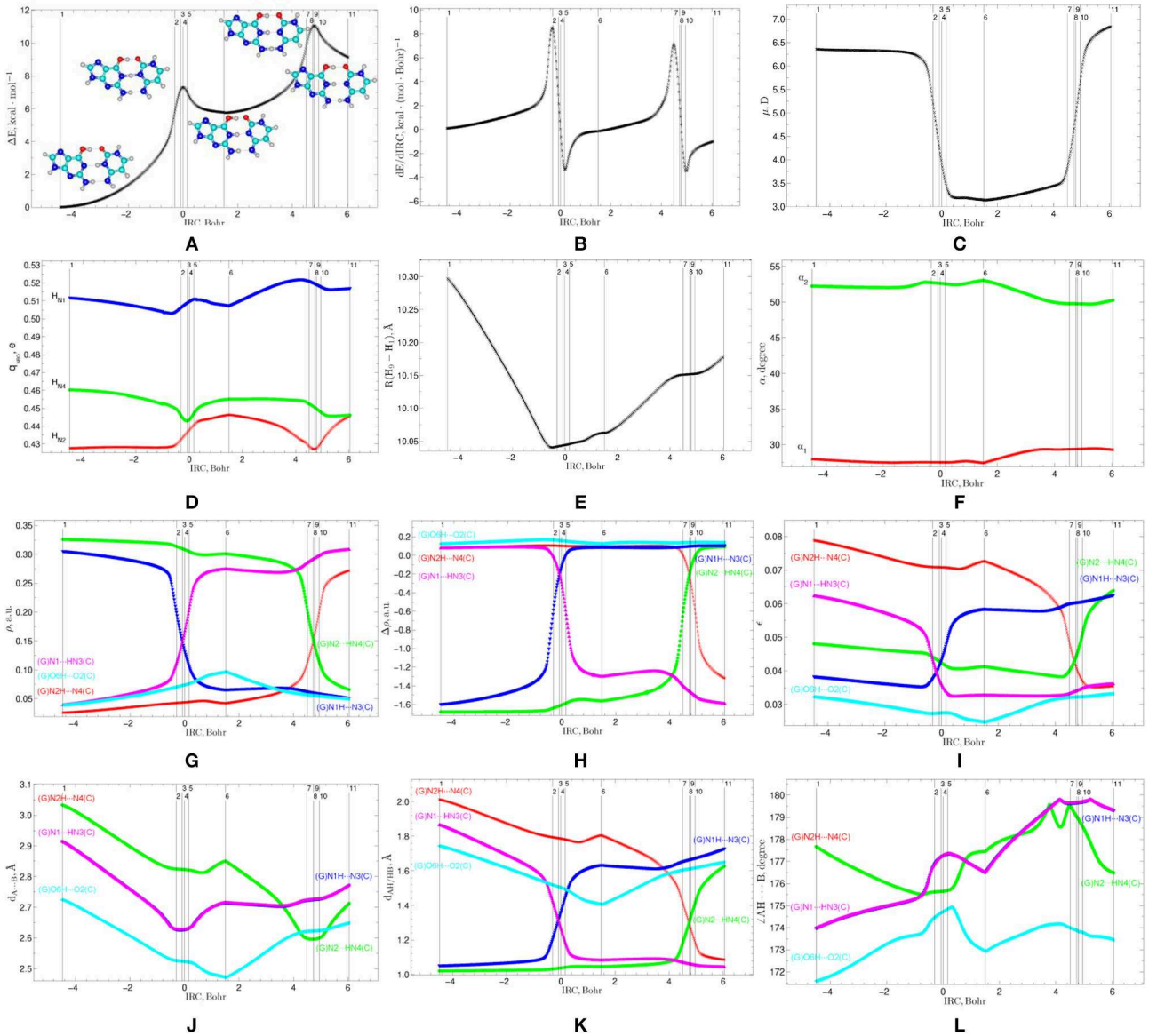

FIGURE 5 | Profiles of physico-chemical parameters of the investigated II. G*·C*(rWC)↔G^{+}·C^{-}(rWC)↔G^{*}_{N2}·C(rWC) tautomerisation *via* the sequential SPT obtained at the B3LYP/6-311++G(d,p) level of theory in vacuum. For more detailed designations see **Figure 3**.

Interaction Energies Calculations

We have obtained electronic interaction energies E_{int} at the MP2/6-311++G(2df,pd) level of theory as the difference between the total electronic energy of the base mispair and the electronic energies of the separate monomers. Gibbs free energy of interaction has been obtained using similar approach. At this, we also corrected the interaction energy for the basis set superposition error (BSSE) (Boys and Bernardi, 1970; Gutowski et al., 1986) according to the counterpoise procedure (Sordo et al., 1988; Sordo, 2001).

Estimation of Kinetic Parameters

The time $\tau_{99.9\%}$ spent for reaching the 99.9% of the equilibrium concentration between the initial and terminal base pairs in the system of reversible first-order forward (k_f) and reverse (k_r) reactions was estimated by formula (Atkins, 1998):

$$\tau_{99.9\%} = \frac{ln10^3}{k_f + k_r}, \tag{2}$$

The lifetime τ of the base pairs was calculated using the formula $1/k_r$, where the values of the reverse k_r and forward k_f rate

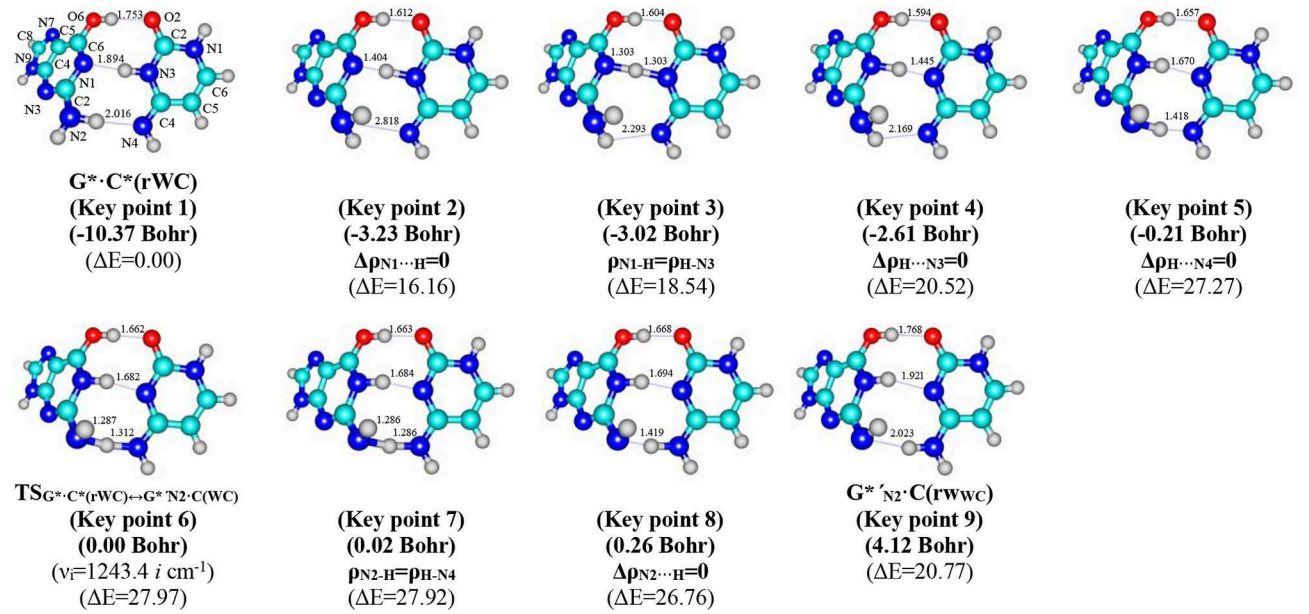

FIGURE 6 | Geometric structures of the 9 key points describing the evolution of the III. G*·C*(rWC)↔G*′$_{N2}$·C(rWC) tautomerisation *via* the DPT along the IRC obtained at the B3LYP/6-311++G(d,p) level of theory *in vacuo* (see **Table 5**). For more detailed designations see **Figure 2**.

constants for the tautomerisation reactions were calculated as (Atkins, 1998):

$$k_{f,r} = \Gamma \cdot \frac{k_B T}{h} e^{-\frac{\Delta\Delta G_{f,r}}{RT}}, \tag{3}$$

where quantum tunneling effects are accounted by Wigner's tunneling correction (Wigner, 1932; Brovarets' and Hovorun, 2014d), that has been successfully used for the DPT reactions (Brovarets' and Hovorun, 2013a,b,c,d, 2014c,d,e, 2015h,i; Brovarets' et al., 2013a,b, 2014a,b,c,d, 2015, 2017):

$$\Gamma = 1 + \frac{1}{24}\left(\frac{h\nu_i}{k_B T}\right)^2, \tag{4}$$

where k_B—Boltzmann's constant, h—Planck's constant, $\Delta\Delta G_{f,r}$—Gibbs free energy for the forward (f) and reverse (r) tautomerisation reactions, ν_i—value of the imaginary frequency at the TS of the tautomerisation reaction.

QTAIM Analysis

Bader's quantum theory of Atoms in Molecules (QTAIM) was used to analyse the electron density distribution (Bader, 1990). The topology of the electron density was analyzed using program package AIMAll (Keith, 2010) with all default options and wave functions obtained at the level of theory used for geometry optimisation. The presence of the (3,−1) bond critical point (BCP), bond path between hydrogen donor and acceptor and positive value of the Laplacian at this BCP ($\Delta\rho > 0$) were considered altogether as criteria for the H-bond formation (Matta and Hernández-Trujillo, 2003; Matta et al., 2006a,b; Matta, 2014; Lecomte et al., 2015; Brovarets' and Pérez-Sánchez, 2016, 2017; Brovarets' et al., 2016).

Energies of the Intermolecular H-Bonds

We calculated the energies of the intermolecular AH···B H-bonds in the base mispairs and TSs and of the sweeps of the H-bond energies by the empirical Espinosa-Molins-Lecomte (EML) formula (Espinosa et al., 1998; Matta et al., 2006b; Mata et al., 2011; Lecomte et al., 2015; Alkorta et al., 2016, 2017) based on the electron density distribution at the (3,−1) BCPs of the H-bonds:

$$E_{AH\cdots B} = 0.5 \cdot \mathrm{V(r)}, \tag{5}$$

where V(r)—value of a local potential energy at the (3,−1) BCP.

EML fomula has been also used for the estimation of the energy of the non-standard H-bonds CH···O in the stationary points of the base pairs on the hypersurface of their electronic energy.

We evaluated the energies of the classical NH···N/O and OH···O/N intermolecular AH···B H-bonds by the empirical Iogansen's formula (Iogansen, 1999):

$$E_{AH\ldots B} = 0.33\sqrt{\Delta\nu - 40}, \tag{6}$$

where $\Delta\nu$–magnitude of the frequency shift of the stretching mode of the AH H-bonded group involved in the AH···B H-bond relatively the unbound group. We applied partial deuteration in order to minimize the effect of vibrational resonances (Brovarets' and Hovorun, 2014d,e, 2015h,i; Brovarets' et al., 2014d).

The energies of the NH· · · N and OH· · · O H-bonds in the TSs containing loosened covalent bridges

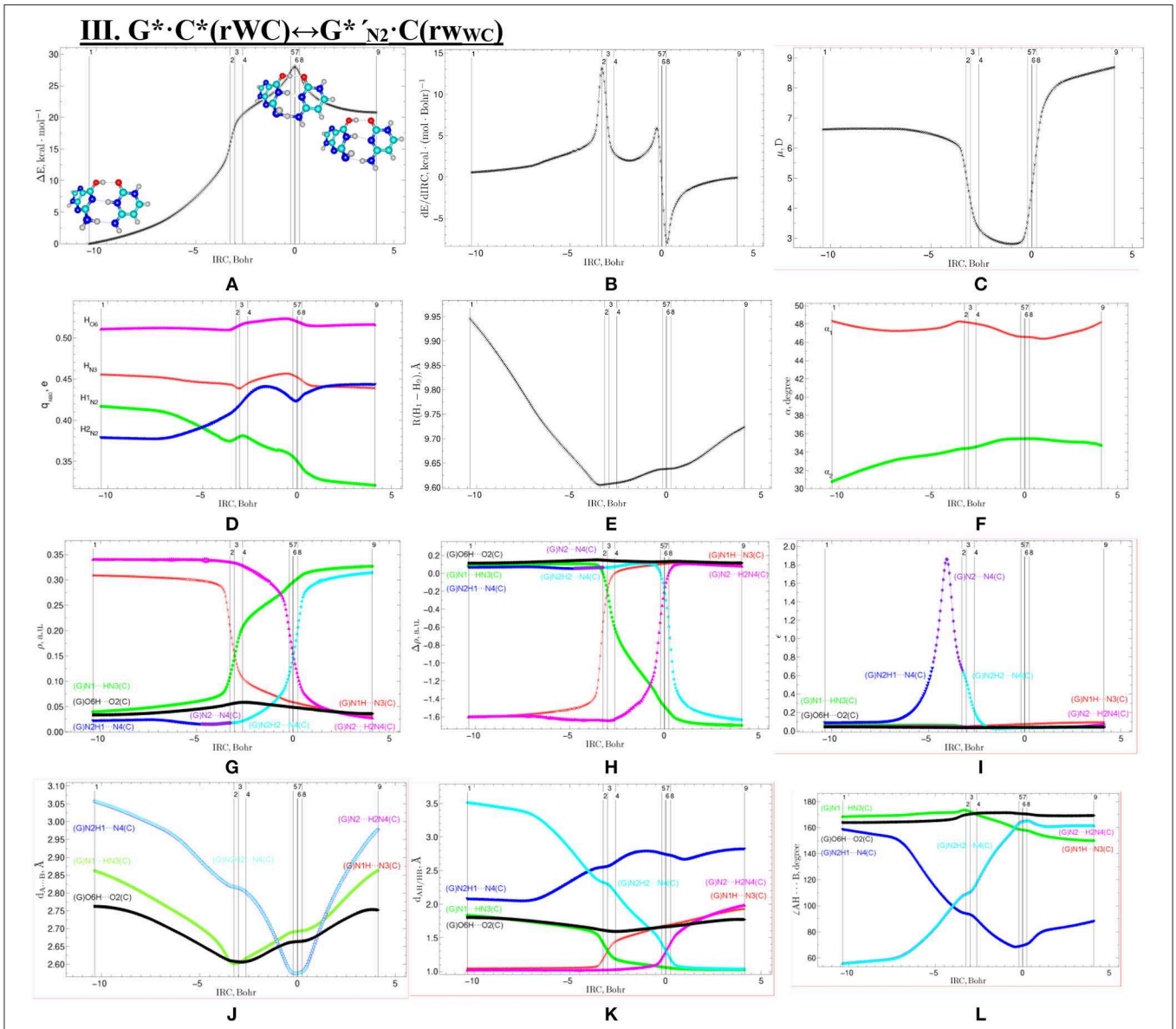

FIGURE 7 | Profiles of the physico-chemical parameters of the investigated III. G*·C*(rWC)↔G*′$_{N2}$·C(rWC) tautomerisation *via* the DPT obtained at the B3LYP/6-311++G(d,p) level of theory in vacuum. For more detailed designations see **Figure 3**.

were calculated by the Nikolaienko-Bulavin-Hovorun formula (Nikolaienko et al., 2012):

$$E_{NH\cdots N} = -2.03 + 225 \cdot \rho, \quad (7)$$

$$E_{OH\cdots O} = -3.09 + 239 \cdot \rho, \quad (8)$$

where ρ–the electron density at the (3,−1) BCP of the H-bond.

The atom numbering scheme for the DNA bases is conventional (Saenger, 1984).

RESULTS AND THEIR DISCUSSION

In this paper we have investigated in details the tautomerisation processes *via* the single (SPT) or double (DPT) proton transfer of the G* · C*(rWC), G*′ · C*(H), and G*′ · C*(rH) base pairs along the neighboring intermolecular H-bonds as their intrinsically inherent property (**Figure 1**).

This paper is organized in the following way—firstly, we would discuss the tautomerisation process separately for each base pair and then we would present in details sweeps of the most important physico-chemical parameters along the IRC altogether for all investigated base pairs (**Figures 1–12**, **Tables 1–8**).

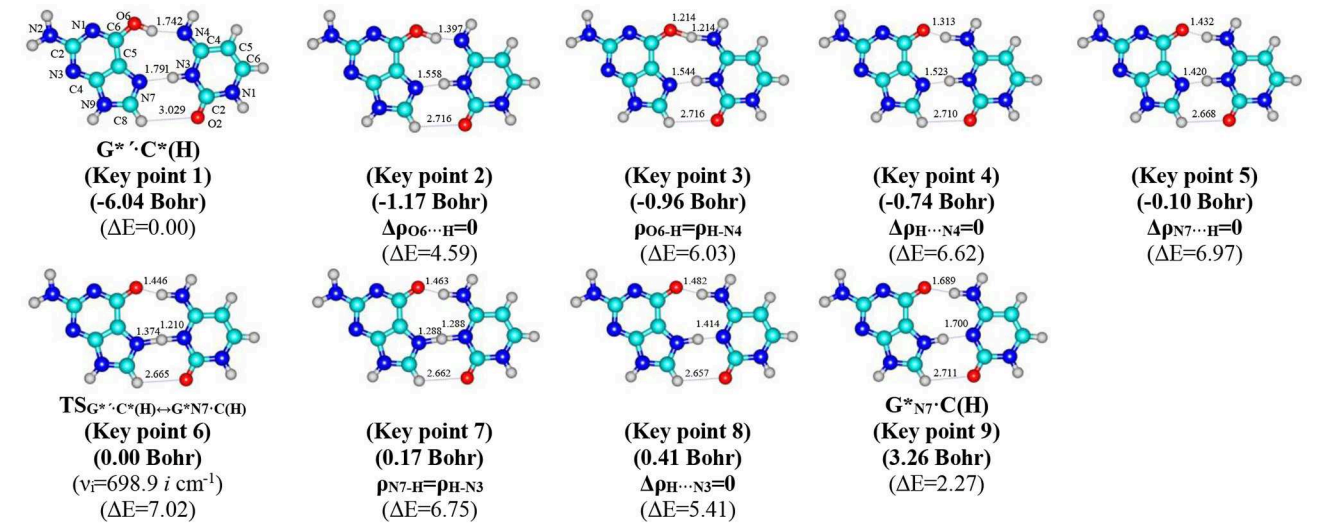

FIGURE 8 | Geometric structures of the 9 key points describing the evolution of the IV. G*′·C*(H)↔G*$_{N7}$·C(H) tautomerisation *via* the DPT along the IRC obtained at the B3LYP/6-311++G(d,p) level of theory *in vacuo* (see **Table 6**). For more detailed designations see **Figure 2**.

Tautomerisation of the Reverse Löwdin G* · C*(rWC) Base Pair *via* the SPT: I. G*·C*(rWC)↔G$^+$·C$^-$(rWC)↔G·C*$_{O2}$(rWC) and II. G*·C*(rWC)↔G$^+$·C$^-$(rWC)↔G*$_{N2}$·C(rWC)

For the first time we have discovered three local minima on the hypersurface of the electronic energy of the G* · C*(rWC) base pair corresponding to the high-energy tautomerised G·C*$_{O2}$(rWC), G$^+$ · C$^-$(rWC), and G*$_{N2}$ · C(rWC) base pairs (**Figure 1**, **Table 1**). All of them are stabilized by the participation of three intermolecular H-bonds, among which the upper O6H…O2/O2H…O6 H-bonds are the strongest (**Table 2**).

In fact, the tautomerisation of the G*·C*(rWC) base pair with relative Gibbs free energy $\Delta G = 0.00$ kcal·mol^{-1} starts from the single transfer of the proton localized at the N3 nitrogen atom of the C base to the N1 nitrogen atom of the G base along the intermolecular H-bond (C)N3H…N1(G). This G*·C*(rWC)↔G$^+$·C$^-$(rWC) tautomerization process occurs *via* the TS$_{G^*\cdot C^*(rWC)\leftrightarrow G^+\cdot C^-(rWC)}$ (C_s symmetry) (ΔG = 4.38 kcal·mol^{-1}) containing N1-H-N3 covalent bridge and further proceeds through the intermediate—tight ion pair G$^+$·C$^-$(rWC) ($\Delta G = 4.44$ kcal·mol^{-1}) (C_s symmetry), which is the point of bifurcation. By the way, it should be noted that this is the first case of the reliable fixation of the ionic pair of bases, formed as a result of the SPT along the intermediate molecular H-bond, which is involved in its stabilization. Similar attempts to localize such structures for the A·T(WC) and G·C(WC) DNA base pairs didn't lead to result.

Further the G*·C*(rWC)↔G$^+$·C$^-$(rWC) tautomerisation reaction proceeds according two scenarios *via* the proton transfer along:

- the (G)O6H….O2(C) H-bond through the TS$_{G^+\cdot C^-(rWC)\leftrightarrow G\cdot C^*O2(rWC)}$ ($\Delta G = 3.64$ kcal·mol^{-1}; C_s symmetry) with O6-H-O2 covalent bridge leading to the G·C*$_{O2}$(rWC) product (C_s symmetry);
- the (G)N2H….N4(C) H-bond through the TS$_{G^+\cdot C^-(rWC)\leftrightarrow G^*N2\cdot C(rWC)}$ ($\Delta G = 9.27$ kcal·mol^{-1}; C_s symmetry) N2-H-N4 covalent bridge leading to the G*$_{N2}$·C(rWC) product (C_s symmetry).

It attracts attention that electronic ΔE_{int} and Gibbs free ΔG_{int} energies of the interaction for the tautomerised G·C*$_{O2}$(rWC) ($\Delta E_{int} = -39.67/\Delta G_{int} = -26.53$) and G*$_{N2}$·C(rWC) ($\Delta E_{int} = -41.10/\Delta G_{int} = -26.10$) base mispairs exceed the values for the initial G*·C*(rWC) base mispair ($\Delta E_{int} = -20.21/\Delta G_{int} = -7.40$) and also canonical G·C(WC) base pair ($\Delta E_{int} = -29.28/\Delta G_{int} = -15.97$ kcal·mol^{-1}) (Brovarets' and Hovorun, 2014a).

Moreover, it was revealed that all three formed high-energy complexes—the G$^+$·C$^-$(rWC) ion pair and G·C*$_{O2}$(rWC), G*$_{N2}$·C(rWC) tautomers of the Löwdin G*·C*(rWC) base pair are dynamically unstable structures, since for them the zero energy of the vibrations, which frequency become imaginary at the TS of tautomerisation, significantly exceeds the reverse electronic barrier (363.8, 668.1, and 454.7 cm^{-1}) (**Table 1**). Moreover, Gibbs free energies of the reverse barrier for the G*·C*(rWC)↔G$^+$·C$^-$(rWC) and G$^+$·C$^-$(rWC)↔G*$_{N2}$·C(rWC) tautomeric transformations are negative (−0.06 and −1.12 kcal·mol^{-1}, accordingly) and for the G$^+$·C$^-$(rWC)↔G·C*$_{O2}$(rWC)—it is less (0.13 kcal·mol^{-1}) than *kT* (0.62 kcal·mol^{-1} under normal conditions) (**Table 1**).

So, in fact the Löwdin G*·C*(rWC) base pair does not tautomerise to the novel G·C*$_{O2}$(rWC) and G*$_{N2}$·C(rWC) base mispairs *via* the SPT along

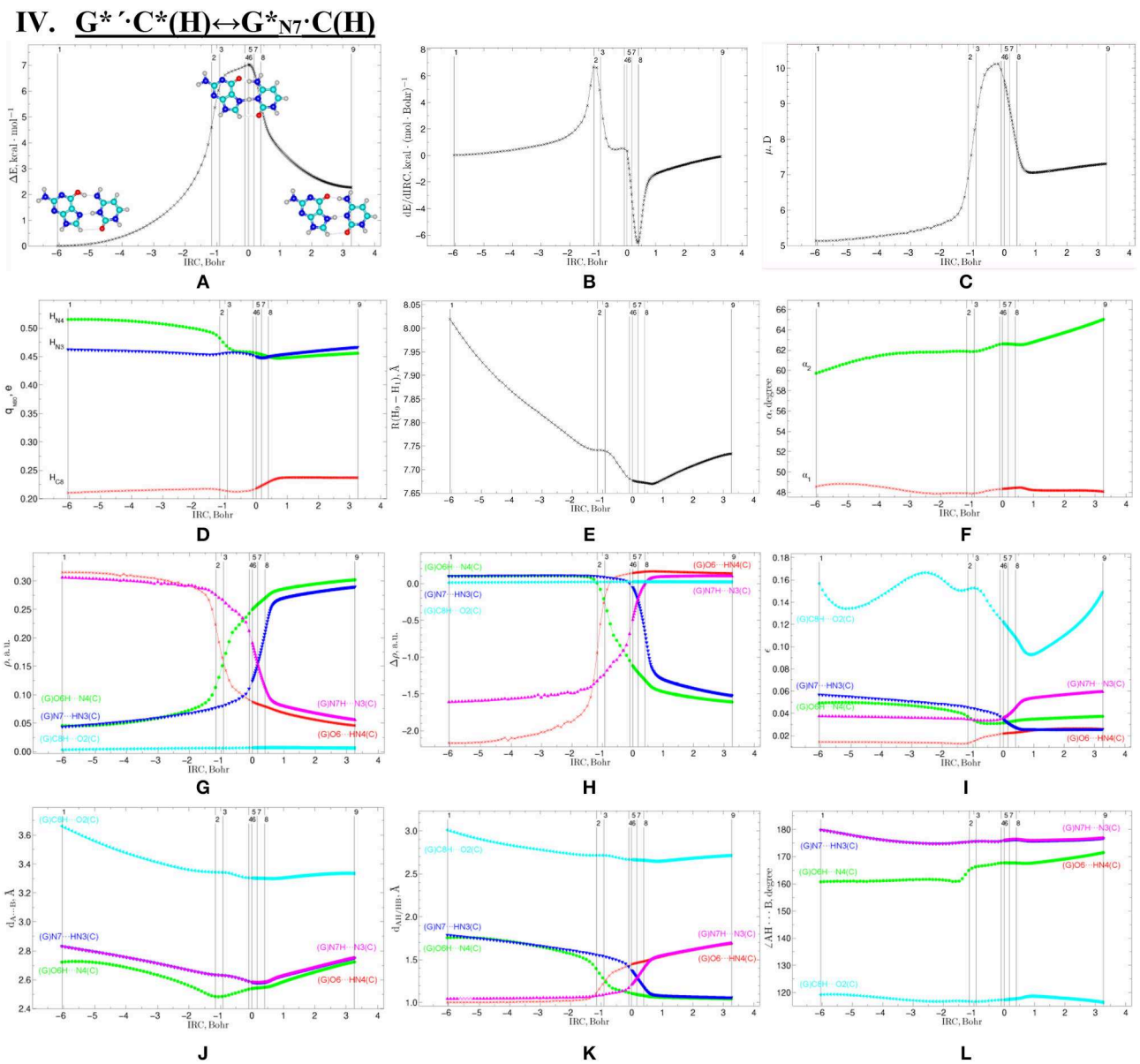

FIGURE 9 | Profiles of the physico-chemical parameters of the investigated IV. G*′·C*(H)↔G*$_{N7}$·C(H) tautomerisation *via* the DPT obtained at the B3LYP/6-311++G(d,p) level of theory in vacuum. For more detailed designations see **Figure 3**.

the intermolecular H-bonds. However, despite this verdict, obtained data can be useful as an analogy or even as a heuristic push at the investigation of the tautomerisation mechanisms of the H-bonded complexes of any nature.

Tautomerisation of the Reverse Löwdin G*·C*(rWC) Base Pair *via* the DPT: III. G*·C*(rWC)↔G*′$_{N2}$·C(rWC)

We have also detected the unusual tautomerisation of the reverse Lowdin's G*·C*(rWC) DNA base mispair *via* the asynchronous [with a level of asynchrony 3.49 Bohr (Brovarets' and Hovorun, 2019b)] concerted DPT to the G*′$_{N2}$·C(rWC) DNA base mispair with *trans*-oriented N2H imino group of the G DNA base, in which participates the protons at the N3(C) and N2(G) nitrogen atoms moving in opposite directions. Unusual nature of this process consists in the fact that the transitions of the protons from N3(C) to N1(G) and from N2(G) to N4(C) along the intermolecular H-bonds provokes the rotation of the NH_2 amino group of the G base into the *trans*-position relatively the neighboring double C2N3(G) bond. As a results, this G*·C*(rWC)↔G*′$_{N2}$·C(rWC) tautomerisation

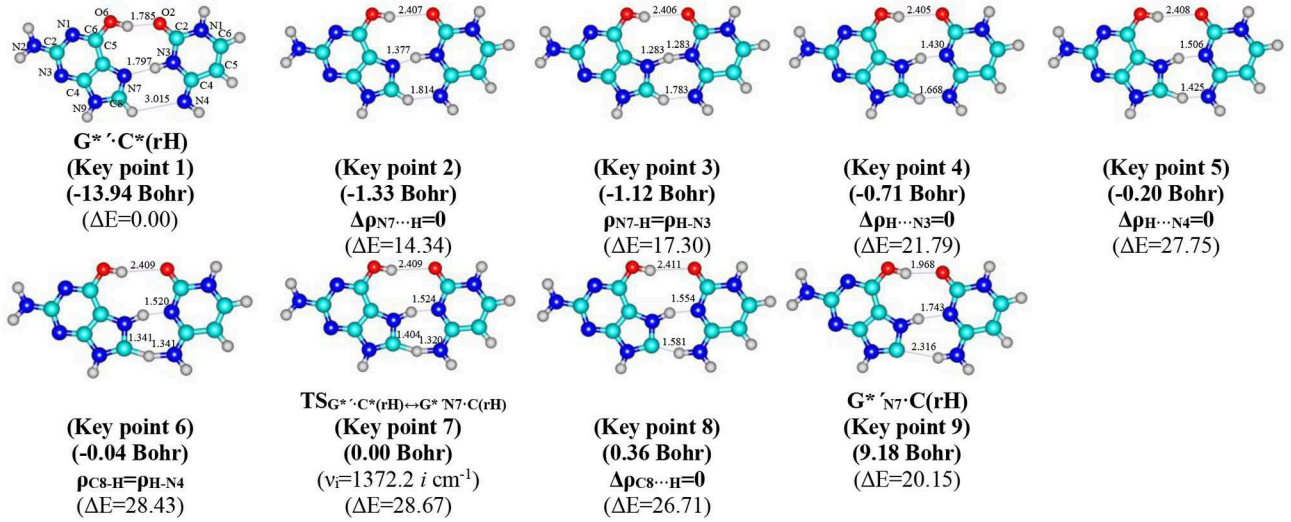

FIGURE 10 | Geometric structures of the 9 key points describing the evolution of the V. G*′·C*(rH)↔G*′$_{N7}$·C(rH) tautomerisation *via* the DPT along the IRC obtained at the B3LYP/6-311++G(d,p) level of theory *in vacuo* (see **Table 7**). For more detailed designations see **Figure 2**.

reaction proceeds through the substantially non-planar intermediate – G$^{+\prime}{}_{N2}$·C^{-}(rWC) ion pair with non-planar NH_2 amino group (C_1 symmetry), the substantially non-planar $TS_{G^{*}\cdot C^{*}(rWC)\leftrightarrow G^{*\prime}N2\cdot C(rWC)}$ (C_1 symmetry), and substantially non-planar product of this reaction—the G*′$_{N2}$·C(rWC) DNA base mispair (C_1 symmetry). This DNA base mispair is stabilized by the participation of the three intermolecular H-bonds—(G)O6H…O2(C), (G)N1H…N3(C), and (C)N4H…N2(G) and represents itself quite stable structure ($\Delta E_{int} = -33.41/\Delta G_{int} = -18.99$ kcal·mol^{-1}). Its characteristic structural feature is the substantial non-flatness (∠N1C6C2N3=23.3°; ∠C2N2N4C4=53.8°) and the exit from the plane of the purine ring of the O6H (∠HO6C6N1=10.8°), N1H (∠HN1C2N3=-157.4°), and N2H (∠HN2C2N3=-167.6°) external groups with the *trans*-orientation relative to the neighboring bond C2N3.

Moreover, we have revealed that the G$^{*}_{N2}$·C(rWC) and G*′$_{N2}$·C(rWC) DNA base pairs interconvert *via* the conformational rotation of the N2H imino group around the C2N2 bond through the Gibbs freee energy barrier 31.65 kcal·mol^{-1} (**Figure 1**, **Tables 1**–**2**).

Tautomerisation of the Hoogsteen G*′·C*(H) Base Pair *via* the Classical DPT: IV. G*′·C*(H)↔G$^{*}_{N7}$·C(H)

The tautomerisation of the Hoogsteen G*′·C*(H) base pair ($\Delta G = 0.00$ kcal·mol^{-1}; C_s symmetry) is possible *via* one-single way—through the asynchronous DPT (the values of the asynchronity consists 1.58 Bohr) (for more details see further discussion and **Figure 8**) along two intermolecular antiparallel lower (G)O6H…N4(C) and (C)N3H…N7(G) H-bonds through the $TS_{G^{*\prime}\cdot C^{*}(H)\leftrightarrow G^{*}N7\cdot C(H)}$ ($\Delta G = 4.01$ kcal·mol^{-1}; C_s symmetry) connected by the N7-H-N3 covalent bridge with further formation of the dynamically-unstable G$^{*}_{N7}$·C(H) base mispair with small lifetime $\tau = 4.46\cdot10^{-13}$ s ($\Delta G = 3.20$ kcal·mol^{-1}; C_s symmetry). The G*′·C*(H)↔G$^{*}_{N7}$·C(H) tautomerisation starts from the initial transfer of the hydrogen atom localized at the O6 oxygen atom of the G*′ DNA base to the N4 nitrogen atom of the C* DNA base within the G*′·C*(H) DNA base pair and then through the G^{+}·C^{-}(H) Hoogsteen base pair *via* the proton transfer from the N3 nitrogen atom to the N7 nitrogen atom leading to the formation of the G$^{*}_{N7}$·C(H) DNA base mispair by the participation of the rare G$^{*}_{N7}$ tautomer and canonical C DNA base.

Notably, that initial and final structures involved in this tautomerisation process are stabilized by the participation of three intermolecular H-bonds (**Table 2**), one of which (G)C8H…O2(C) is non-standard with energy 1.15 kcal·mol^{-1}.

Notably, electronic ($\Delta E_{int} = -35.66$) and Gibbs free ($\Delta G_{int} = -22.05$ kcal·mol^{-1}) energies of the interaction for the terminal G$^{*}_{N7}$·C(H) base mispair exceed the values for the initial base mispair ($\Delta E_{int} = -21.24/\Delta G_{int} = -8.91$ kcal·mol^{-1}). At this, total energies of the H-bonds make a great contribution to the electronic interaction energy—78.1% for the G*′·C*(H) DNA base mispair and 51.7% for the G$^{*}_{N7}$·C(H) DNA base mispair.

All low-frequency intermolecular vibrations of the G$^{*}_{N7}$·C(H) base mispair, which periods are in the range $8.06\cdot10^{-13}$-$1.16\cdot10^{-12}$ s, can't develop during its lifetime. This situation is typical for the structures, which are deprived of dynamic stability (Brovarets' and Hovorun, 2019b).

So, in this case in fact the G*′·C*(H) base pair does not tautomerise *via* the DPT similarly to the previous G*·C*(rWC) base pair.

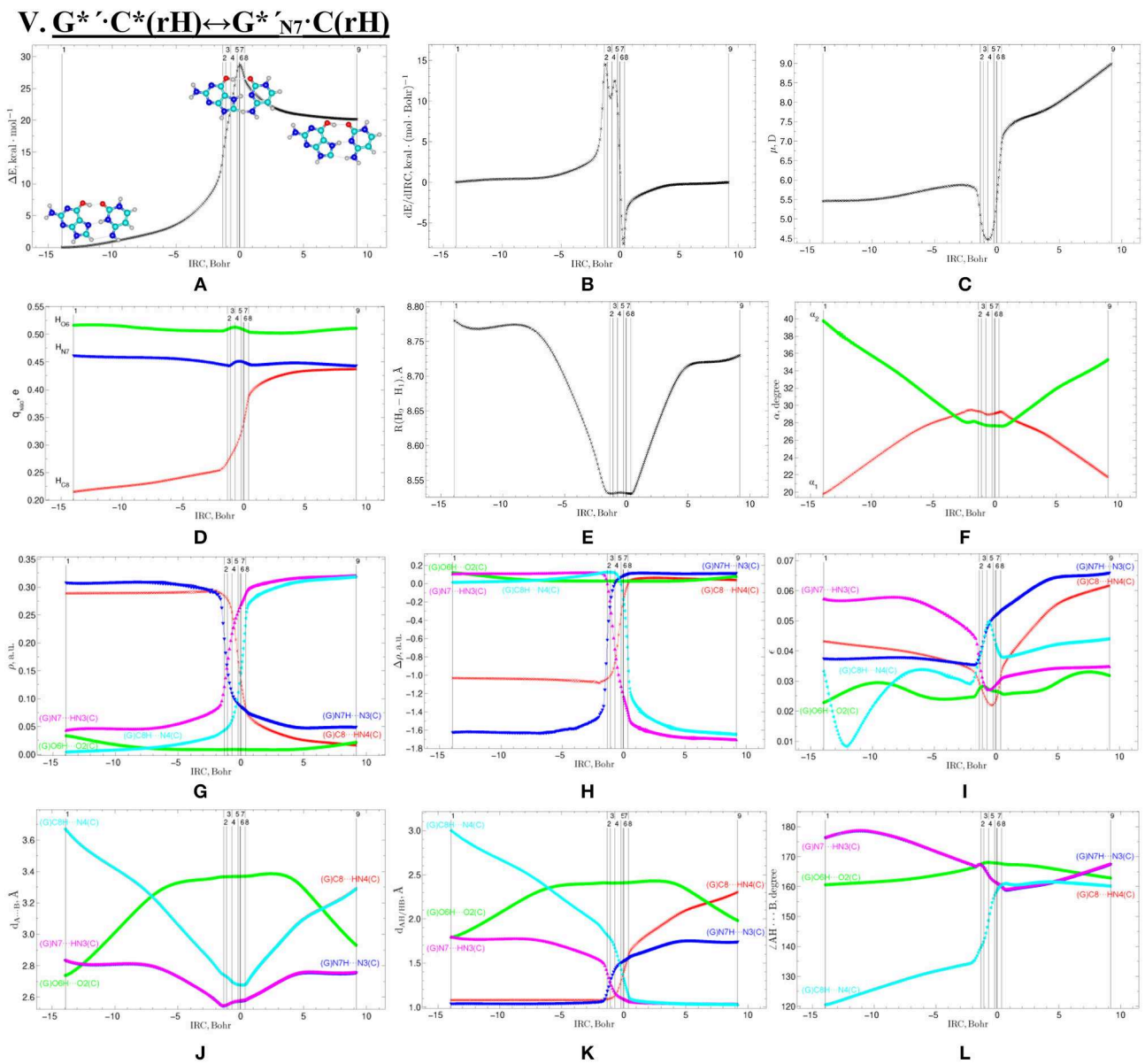

FIGURE 11 | Profiles of the physico-chemical parameters of the investigated V. G*′·C*(rH)↔G*′$_{N7}$·C(rH) tautomerisation *via* the DPT obtained at the B3LYP/6-311++G(d,p) level of theory in vacuum. For more detailed designations see **Figure 3**.

Tautomerisation of the Reverse Hoogsteen G*′·C*(rH) Base Pair *via* the DPT by the Participation of the C8H(G*′) Group: V. G*′·C*(rH)↔G*′$_{N7}$·C(rH)

The G*′·C*(rH) base pair differs from two previous ones, since it tautomerises *via* the asynchronous DPT (with the value of asynchronity 1.69 Bohr) along the intermolecular antiparallel (C)N3H…N7(G) and (G)C8H…N4(C) H-bonds with further formation of the yilidic form G*′$_{N7}$ of the G DNA base (Govorun et al., 1995a,b; Kondratyuk et al., 2000), which is characterized by the transferred proton of the C8H group to the neighboring N7 nitrogen atom. The G*′·C*(rH)↔G*′$_{N7}$·C(rH) tautomerisation proceeds *via* the initial transfer of the proton localized at the N3 nitrogen atom of C base to the N7 nitrogen atom of G base through the formation of the G$^{+\prime}{}_{N7}$·C^{-} ion pair followed by further proton transfer localized at the C8 carbon atom of G*′ base to the N4 nitrogen atom of C* base. Notably, that TS of this process—TS$_{G^{*\prime}\cdot C^{*}(rH)\leftrightarrow G^{*\prime}N7\cdot C(rH)}$–has planar structure ($C_s$ symmetry) and contains C8-H-N4 covalent bridge, which angle is 158.8°.

This process is become possible due to the fact that G base, from one side, is CH-acid (Kondratyuk et al., 2000) and from the

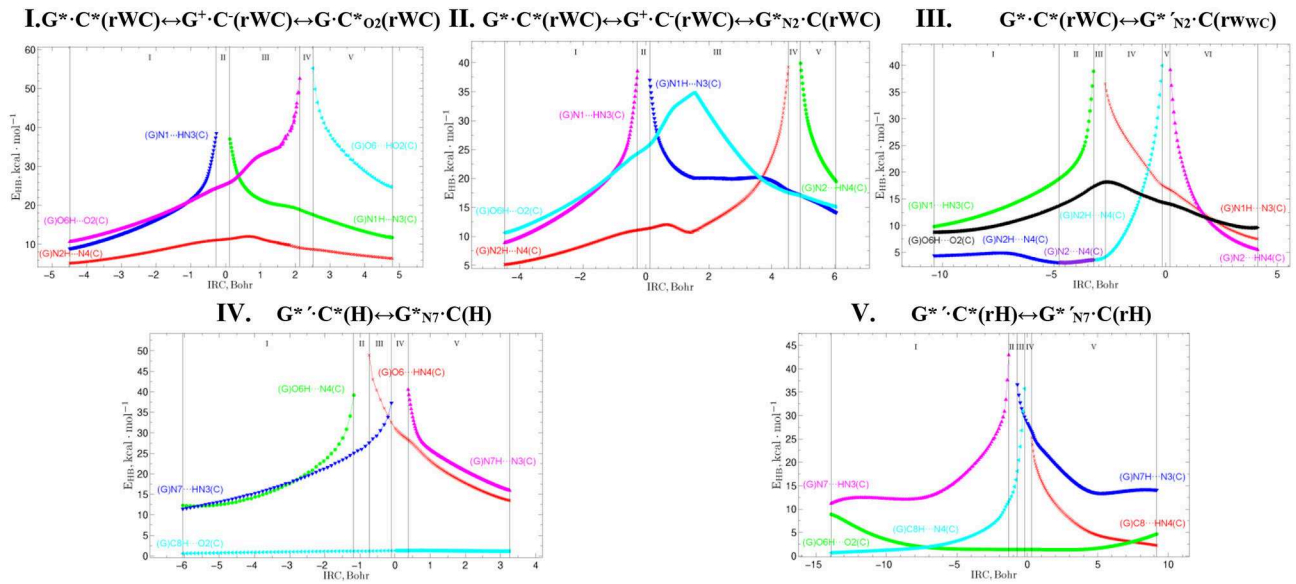

FIGURE 12 | Profiles of the energy of the intermolecular H-bonds E_{HB} estimated by the EML formula at the (3,−1) BCPs along the IRC of the investigated tautomerisations *via* the SPT or DPT obtained at the B3LYP/6-311++G(d,p) level of theory (see **Table 3**).

TABLE 1 | Energetic (in kcal·mol^{-1}) and kinetic (in s) characteristics of the tautomerisation of the G*·C*(rWC), G$^{*'}$·C*(H), and G$^{*'}$·C*(rH) DNA base pairs *via* the SPT or DPT obtained at the MP2/aug-cc-pVDZ//B3LYP/6-311++G(d,p) level of QM theory in the continuum with ε = 1 under normal conditions (see **Figure 1**).

Tautomeric transition	ν_i^a	ΔG^b	ΔE^c	$\Delta\Delta G^d_{TS}$	$\Delta\Delta E^e_{TS}$	$\Delta\Delta G^f$	$\Delta\Delta E^g$		$\tau^h_{99.9\%}$	τ^i
							kcal·mol^{-1}	cm^{-1}		
G*·C*(rWC)↔G$^+$·C$^-$(rWC)	1132.1	4.44	5.68	4.38	6.72	−0.06	1.04	363.8	$4.70\cdot10^{-13}$	$6.80\cdot10^{-14}$
G$^+$·C$^-$(rWC)↔G·C*$_{O2}$(rWC)	383.9	−0.93	−1.88	−0.80	0.03	0.13	1.91	668.1	$2.10\cdot10^{-13}$	$1.77\cdot10^{-13}$
G$^+$·C$^-$(rWC)↔G*$_{N2}$·C(rWC)	1104.5	5.95	4.56	4.83	5.87	−1.12	1.30	454.7	$7.96\cdot10^{-14}$	$1.15\cdot10^{-14}$
G*·C*(rWC)↔G*′$_{N2}$·C(rWC)	1243.4	24.74	24.58	27.43	29.29	2.69	4.71	1647.6	$4.39\cdot10^{-11}$	$6.35\cdot10^{-12}$
G*$_{N2}$·C(rWC)↔G*′$_{N2}$·C(rWC)	663.5	14.35	14.34	21.25	22.57	6.90	8.23	2878.9	$9.24\cdot10^{-8}$	$1.34\cdot10^{-8}$
G*′·C*(H)↔G*$_{N7}$·C(H)	675.7	3.20	3.07	4.01	6.65	0.81	3.58	1252.3	$3.07\cdot10^{-12}$	$4.46\cdot10^{-13}$
G*′·C*(rH)↔G*′$_{N7}$·C(rH)	1326.7	22.69	22.35	25.30	28.76	2.61	6.41	2242.2	$3.56\cdot10^{-11}$	$5.15\cdot10^{-12}$

[a] *The imaginary frequency at the TS of the tautomeric transition, cm^{-1}.*
[b] *The Gibbs free energy of the initial relatively the terminal base pair of the tautomerisation reaction (T = 298.15 K).*
[c] *The electronic energy of the initial relatively the terminal base pair of the tautomerisation reaction.*
[d] *The Gibbs free energy barrier for the forward tautomerisation reaction.*
[e] *The electronic energy barrier for the forward tautomerisation reaction.*
[f] *The Gibbs free energy barrier for the reverse tautomerisation reaction.*
[g] *The electronic energy barrier for the reverse tautomerisation reaction.*
[h] *The time necessary to reach 99.9% of the equilibrium concentration between the reactant and the product of the tautomerisation reaction.*
[i] *The lifetime of the product of the tautomerisation reaction.*

other—it is able to transfer into the zwitterionic tautomer—so-called yilidic form (Govorun et al., 1995a,b; Kondratyuk et al., 2000). Analysis of the obtained data (**Table 1**) evidences that G*′$_{N7}$·C(rH) tautomer is dynamically stable structure with quite long lifetime ($\tau = 5.15\cdot10^{-12}$ s). Characteristically, that all 6 low-frequency intermolecular vibrations of the G*′$_{N7}$·C(rH) base mispair, which period are in the range $6.83\cdot10^{-13}$-$1.51\cdot10^{-12}$ s, can develop during this lifetime.

This is the first case (Brovarets' et al., 2018f), when the product of the tautomerization of the H-bonded base pair by the participation of the yilidic purine base is dynamically stable structure. However, formed G*′$_{N7}$·C(rH) base pair has low population—$2.3\cdot10^{-17}$ under normal conditions, which complicates the understanding of its biological role.

At the same time, such structures represent a considerable interest from a theoretical point of view, in particular, they contain unusual (C)N4H…C8$^-$(G) H-bond (**Table 2**), which supplements existing data about the nature of the H-bonding in the pairs of DNA/RNA bases (Brovarets' et al., 2014e).

TABLE 2 | Electron-topological, geometrical, and energetic characteristics of the intermolecular H-bonds in the investigated DNA base pairs in rare tautomeric forms and TSs of their tautomerization *via* the SPT or DPT obtained at the B3LYP/6-311++G(d,p) level of QM theory (ε = 1) (see **Figure 1**).

Complex	AH···B H–bond	ρ^a	$\Delta\rho^b$	$100 \cdot \varepsilon^c$	$d^d_{A\cdots B}$	$d^e_{H\cdots B}$	$\angle AH \cdots B^f$	$\Delta\upsilon^g$	$EAH\cdots B^h$	μ^i
G*·C*(rWC)↔G$^+$·C$^-$(rWC)										
G*·C*(rWC) (Brovarets', 2013b)	O6H· · ·O2	0.038	0.124	3.31	2.731	1.753	171.1	359.4	5.90	6.54
	N3H· · ·N1	0.035	0.086	6.32	2.932	1.894	173.6	538.2	7.37	
	N2H· · ·N4	0.026	0.077	8.04	3.036	2.016	178.0	248.9	4.77	
$TS_{G^*\cdot C^*(rWC)\leftrightarrow G^+\cdot C^-(rWC)}$	O6H· · ·O2	0.074	0.158	2.77	2.525	1.505	174.9	–	14.60**	3.92
	N2H· · ·N4	0.043	0.102	7.06	2.829	1.793	175.2	–	7.64**	
$G^+\cdot C^-$(rWC)	$O6^+H\cdot\cdot\cdot O2^-$	0.103	0.113	2.40	2.458	1.384	172.4	1764.1	13.70	3.20
	$N1^+H\cdot\cdot\cdot N3^-$	0.064	0.091	5.91	2.726	1.649	176.0	1092.3	10.70	
	$N2^+H\cdot\cdot\cdot N4^-$	0.041	0.094	7.36	2.860	1.816	177.4	665.6	8.25	
I. G$^+$·C$^-$(rWC)↔G·C*$_{O2}$(rWC)										
$TS_{G^+\cdot C^-(rWC)\leftrightarrow G\cdot C^*O2(rWC)}$	N1H· · ·N3	0.059	0.097	5.98	2.740	1.676	174.6	–	11.01**	3.45
	N2H· · ·N4	0.037	0.091	7.54	2.899	1.860	176.6	–	6.30**	
$G\cdot C^*_{O2}$(rWC)	O2H· · ·O6	0.074	0.150	2.00	2.532	1.500	173.7	1237.6	11.42	5.43
	N1H· · ·N3	0.041	0.099	6.25	2.856	1.825	171.8	465.8	6.81	
	N2H· · ·N4	0.029	0.082	7.83	2.987	1.961	174.7	368.5	5.98	
II. G$^+$·C$^-$(rWC)↔G*$_{N2}$·C(rWC)										
$TS_{G^+\cdot C^-(rWC)\leftrightarrow G^*N2\cdot C(rWC)}$	O6H· · ·O2	0.056	0.139	3.20	2.621	1.611	173.6	–	10.29**	4.99
	N1H· · ·N3	0.059	0.103	6.10	2.733	1.676	179.9	–	11.25**	
$G^*_{N2}\cdot C$(rWC)	O6H· · ·O2	0.047	0.134	3.32	2.666	1.670	172.7	684.4	8.38	7.15
	N1H· · ·N3	0.042	0.101	6.53	2.851	1.815	179.0	455.4	6.73	
	N4H· · ·N2	0.048	0.094	7.08	2.816	1.756	176.4	846.1	9.37	
III. G*·C*(rWC)↔G*′$_{N2}$·C(rWC)										
$TS_{G^*\cdot C^*(rWC)\leftrightarrow G^{*\prime}N2\cdot C(rWC)}$	O6H· · ·O2	0.049	0.131	3.84	2.663	1.662	170.6	–	10.29**	4.55
	N1H· · ·N3	0.059	0.105	7.29	2.692	1.682	158.2	–	11.25**	
$G^{*\prime}_{N2}\cdot C$(rWC)	O6H· · ·O2	0.037	0.117	3.87	2.750	1.768	170.4	503.5	6.98	8.85
	N1H· · ·N3	0.033	0.095	8.50	2.876	1.921	153.8	243.0	4.61	
	N4H· · ·N2	0.024	0.071	11.36	3.014	2.023	160.2	409.3	6.22	
$TS_{G^*N2\cdot C(rWC)\leftrightarrow G^{*\prime}N2\cdot C(rWC)}$	O6H· · ·O2	0.048	0.132	3.59	2.665	1.666	172.2	766.7	8.74	5.92
	N1H· · ·N3	0.045	0.105	7.02	2.805	1.787	165.5	504.7	6.98	
	N4H· · ·N2	0.058	0.082	5.23	2.759	1.681	173.4	1291.9	11.47	
IV. G*′·C*(H)↔G*$_{N7}$·C(H)										
G*′·C*(H) (Brovarets', 2013b)	O6H· · ·N4	0.047	0.102	4.88	2.710	1.742	160.7	691.6	8.42	5.16
	N3H· · ·N7	0.032	0.101	5.68	2.834	1.791	180.0	572.6	7.62	
	C8H· · ·O2	0.003	0.012	1.73	3.675	3.029	118.9	−4.1	0.55*	
$TS_{G^{*\prime}\cdot C^*(H)\leftrightarrow G^*N7\cdot C(H)}$	N4H· · ·O6	0.088	0.143	2.19	2.539	1.446	167.7	–	17.77**	9.63
	C8H· · ·O2	0.007	0.024	12.24	3.303	2.665	117.4	–	1.27*	
$G^*_{N7}\cdot C$(H)	N4H· · ·O6	0.045	0.137	2.53	2.728	1.689	172.2	13.2	8.03	7.32
	N7H· · ·N3	0.054	0.099	5.95	2.758	1.700	177.2	15.5	9.26	
	C8H· · ·O2	0.006	0.022	16.54	3.324	2.711	115.8	1.2	1.15*	
V. G*′·C*(rH)↔G*′$_{N7}$·C(rH)										
G*′·C*(rH) (Brovarets', 2013b)	O6H· · ·O2	0.034	0.120	2.25	2.733	1.785	160.6	319.0	5.51	5.43
	N3H· · ·N7	0.042	0.101	2.73	2.838	1.797	176.3	535.6	7.35	
	C8H· · ·N4	0.004	0.013	3.58	3.681	3.015	120.4	−2.1	0.63*	
$TS_{G^{*\prime}\cdot C^*(rH)\leftrightarrow G^{*\prime}N7\cdot C(rH)}$	O6H· · ·O2	0.009	0.027	2.66	3.368	2.409	167.9	–	1.36**	5.52
	N7H· · ·N3	0.086	0.087	5.18	2.576	1.524	161.1	–	17.32**	
$G^{*\prime}_{N7}\cdot C$(rH)	O6H· · ·O2	0.022	0.080	3.15	2.918	1.968	162.9	112.6	2.81	9.01
	N7H· · ·N3	0.049	0.114	6.60	2.758	1.743	167.8	619.6	7.94	
	$N4H\cdot\cdot\cdot C8^-$	0.016	0.038	6.19	3.302	2.316	160.1	339.7	5.71	

[a] *The electron density at the (3,−1) BCP of the H-bond, a.u.*
[b] *The Laplacian of the electron density at the (3,−1) BCP of the H-bond, a.u.*
[c] *The ellipticity at the (3,−1) BCP of the H-bond.*
[d] *The distance between the A and B atoms of the AH···B H-bond, Å.*
[e] *The distance between the H and B atoms of the AH···B H-bond, Å.*
[f] *The H-bond angle, degree.*
[g] *The redshift of the stretching vibrational mode ν(AH) of the AH H-bonded group, cm^{-1}.*
[h] *Energy of the H-bonds, calculated by Iogansen's (Iogansen, 1999), Espinose-Molins-Lecomte (Espinosa et al., 1998; Matta et al., 2006b; Mata et al., 2011; Lecomte et al., 2015; Alkorta et al., 2016, 2017) (marked with an asterisk), or Nikolaienko-Bulavin-Hovorun (Nikolaienko et al., 2012) (marked with a double asterisk) formulas, kcal·mol^{-1}.*
[i] *The dipole moment of the complex, D.*

TABLE 3 | Electron-topological and structural characteristics of the specific intermolecular bonds revealed in the 11 key points and the polarity of the latters along the IRC of the I. G*·C*(rWC)↔G^+·C^-(rWC)↔G·C^*_{O2}(rWC) tautomerisation obtained at the B3LYP/6-311++G(d,p) level of theory in vacuum (see **Figure 2**).

Complex	AH· · · B H-bond/ A-H/H-B covalent bond	ρ[a]	$\Delta\rho$[b]	$100 \cdot \varepsilon$[c]	$d^d_{A\cdots B}$	$d^e_{H\cdots B}$	$\angle AH\cdots B$[f]	μ[g]
Key point 1 (−4.49 Bohr): G*·C*(rWC)	O6H···O2	0.038	0.124	3.31	2.731	1.753	171.1	6.54
	N1···HN3	0.035	0.086	6.32	2.932	1.894	173.6	
	N2H···N4	0.026	0.077	8.04	3.036	2.016	178.0	
Key point 2 (−0.31 Bohr): $\Delta\rho_{N1\cdots H}=0$	O6H···O2	0.070	0.166	2.75	2.528	1.520	174.6	5.19
	N1···HN3	0.110	0.000	4.31	2.621	1.427	176.7	
	N2H···N4	0.042	0.105	7.07	2.831	1.801	175.2	
Key point 3 (−0.08 Bohr): $\rho_{N1-H}=\rho_{H-N3}$	O6H···O2	0.073	0.160	2.76	2.526	1.509	174.9	4.23
	N1-H/H-N3	0.148	−0.193	3.73	2.620	1.310	177.0	
	N2H···N4	0.043	0.103	7.06	2.829	1.795	175.2	
Key point 4 (0.00 Bohr): $TS_{G^*\cdot C^*(rWC)\leftrightarrow G+\cdot C-(rWC)}$	O6H···O2	0.074	0.158	2.76	2.525	1.505	174.9	3.92
	N1-HN3	0.166	−0.306	3.58	2.621	1.268	177.1	
	N1H-N3	0.133	−0.111	4.28	2.621	1.354	177.1	
	N2H···N4	0.043	0.102	7.06	2.829	1.793	175.2	
Key point 5 (0.16 Bohr): $\Delta\rho_{H\cdots N3}=0$	O6H···O2	0.076	0.152	2.77	2.523	1.494	175.0	3.45
	N1H···N3	0.107	0.004	4.75	2.625	1.439	177.1	
	N2H···N4	0.044	0.100	7.05	2.827	1.788	175.3	
Key point 6 (1.50 Bohr): $G^+\cdot C^-$(rWC)	O6H···O2	0.096	0.126	2.50	2.459	1.384	173.1	3.15
	N1H···N3	0.067	0.089	5.79	2.731	1.649	176.3	
	N2H···N4	0.042	0.095	7.24	2.861	1.816	177.0	
Key point 7 (2.13 Bohr): $\Delta\rho_{H\cdots O2}=0$	O6H···O2	0.130	0.006	2.13	2.421	1.298	171.9	3.35
	N1H···N3	0.060	0.096	5.97	2.738	1.672	174.7	
	N2H···N4	0.037	0.091	7.53	2.897	1.858	176.6	
Key point 8 (2.20 Bohr): $TS_{G^+\cdot C^-(rWC)\leftrightarrow G\cdot C^*O2(rWC)}$	O6H-O2	0.138	−0.045	2.05	2.416	1.275	171.9	3.45
	O6-HO2	0.199	−0.644	1.34	2.416	1.147	171.9	
	N1H···N3	0.059	0.097	5.98	2.740	1.676	174.6	
	N2H···N4	0.037	0.091	7.54	2.899	1.860	176.6	
Key point 9 (2.32 Bohr): $\rho_{O6-H}=\rho_{H-O2}$	O6-H/H-O2	0.172	−0.334	1.43	2.409	1.196	172.0	3.77
	N1H···N3	0.058	0.100	6.00	2.743	1.686	174.4	
	N2H···N4	0.037	0.091	7.56	2.902	1.865	176.6	
Key point 10 (2.51 Bohr): $\Delta\rho_{O6\cdots H}=0$	O6···HO2	0.134	−0.006	1.63	2.411	1.286	172.0	4.48
	N1H···N3	0.056	0.104	6.01	2.747	1.698	174.3	
	N2H···N4	0.036	0.092	7.57	2.904	1.870	176.6	
Key point 11 (4.75 Bohr): G·C^*_{O2}(rWC)	O6···HO2	0.074	0.150	2.00	2.532	1.500	173.7	5.43
	N1H···N3	0.041	0.099	6.25	2.856	1.825	171.8	
	N2H···N4	0.029	0.082	7.83	2.987	1.961	174.7	

[a] *The electron density at the (3,−1) BCP, a.u.*
[b] *The Laplacian of the electron density at the (3,−1) BCP, a.u.*
[c] *The ellipticity at the (3–1) BCP.*
[d] *The distance between the A (H-bond donor) and B (H-bond acceptor) atoms of the H-bonds, Å.*
[e] *The distance between the H and B atoms of the H-bonds, Å.*
[f] *The H-bond angle, degree.*
[g] *The dipole moment of the complex, D.*

Profiles of the Physico-Chemical Parameters of the Investigated SPT and DPT Tautomerisations

We have investigated in details the mechanisms of the abovementioned processes of the tautomerisation of the reverse Lowdin's G*·C*(rWC), Hoogsteen G*′·C*(H), and reverse Hoogsteen G*′·C*(rH) base pairs *via* the PT along the intermolecular H-bonds. Tautomerisations proceed in *a synchronous concerted manner via the stepwise SPT* in the case of the I. G*·C*(rWC)↔G^+·C^-(rWC)↔G·C^*_{O2}(rWC) and II. G*·C*(rWC)↔G^+·C^-(rWC)↔G^*_{N2}·C(rWC) reactions, while in *an asynchronous concerted manner via the DPT* in the case of the

TABLE 4 | Electron-topological and structural characteristics of the specific intermolecular bonds revealed in the 11 key points and the polarity of the latters along the IRC of the II. G*·C*(rWC)↔G^{+}·C^{-}(rWC)↔G^{*}_{N2}·C(rWC) tautomerisation obtained at the B3LYP/6-311++G(d,p) level of theory in vacuum (see **Figure 4**).

Complex	AH· · · B H-bond/A-H/H-B covalent bond	ρ^a	$\Delta\rho^b$	$100 \cdot \varepsilon^c$	$d^d_{A\cdots B}$	$d^e_{H\cdots B}$	$\angle_{AH\cdots B}{}^f$	μ^g
Key point 1 (−4.49 Bohr): G*·C*(rWC)	O6H···O2	0.038	0.124	3.31	2.731	1.753	171.1	6.54
	N1···HN3	0.035	0.086	6.32	2.932	1.894	173.6	
	N2H···N4	0.026	0.077	8.04	3.036	2.016	178.0	
Key point 2 (−0.31 Bohr): $\Delta\rho_{N1\cdots H} = 0$	O6H···O2	0.070	0.166	2.75	2.528	1.520	174.6	5.19
	N1···HN3	0.110	0.000	4.31	2.621	1.427	176.7	
	N2H···N4	0.042	0.105	7.07	2.831	1.801	175.2	
Key point 3 (−0.08 Bohr): $\rho_{N1-H} = \rho_{H-N3}$	O6H···O2	0.073	0.160	2.76	2.526	1.509	174.9	4.23
	N1-H/H-N3	0.148	−0.193	3.73	2.620	1.310	177.0	
	N2H···N4	0.043	0.103	7.06	2.829	1.795	175.2	
Key point 4 (0.00 Bohr): $TS_{G^{*}\cdot C^{*}(rWC)\leftrightarrow G^{+}\cdot C^{-}(rWC)}$	O6H···O2	0.074	0.158	2.76	2.525	1.505	174.9	3.92
	N1-HN3	0.166	−0.306	3.58	2.621	1.268	177.1	
	N1H-N3	0.133	−0.111	4.28	2.621	1.354	177.1	
	N2H···N4	0.043	0.102	7.06	2.829	1.793	175.2	
Key point 5 (0.16 Bohr): $\Delta\rho_{H\cdots N3} = 0$	O6H···O2	0.076	0.152	2.77	2.523	1.494	175.0	3.45
	N1H···N3	0.107	0.004	4.75	2.625	1.439	177.1	
	N2H···N4	0.044	0.100	7.05	2.827	1.788	175.3	
Key point 6 (1.50 Bohr): $G^{+}\cdot C^{-}$(rWC)	O6H···O2	0.096	0.126	2.50	2.449	1.384	173.1	3.15
	N1H···N3	0.067	0.089	5.79	2.731	1.649	176.3	
	N2H···N4	0.042	0.095	7.24	2.861	1.814	177.0	
Key point 7 (4.51 Bohr): $\Delta\rho_{N2\cdots H} = 0$	O6H···O2	0.057	0.136	3.19	2.620	1.603	173.8	3.91
	N1H···N3	0.061	0.096	6.06	2.731	1.663	179.8	
	N2H···N4	0.112	−0.001	4.86	2.592	1.409	180.0	
Key point 8 (4.73 Bohr): $\rho_{N2-H} = \rho_{H-N4}$	O6H···O2	0.056	0.138	3.20	2.621	1.609	173.7	4.72
	N1H···N3	0.059	0.102	6.09	2.733	1.673	179.9	
	N2-H/H-N4	0.152	−0.211	4.15	2.590	1.294	179.4	
Key point 9 (4.79 Bohr): $TS_{G^{+}\cdot C^{-}(rWC)\leftrightarrow G^{*}N2\cdot C(rWC)}$	O6H···O2	0.056	0.139	3.21	2.621	1.611	173.6	4.99
	N1H···N3	0.059	0.103	6.10	2.733	1.676	179.9	
	N2-HN4	0.139	−0.130	4.59	2.591	1.329	179.3	
	N2H-N4	0.165	−0.300	4.01	2.591	1.262	179.3	
Key point 10 (4.96 Bohr): $\Delta\rho_{H\cdots N4} = 0$	O6H···O2	0.055	0.140	3.21	2.622	1.615	173.6	5.74
	N1H···N3	0.058	0.106	6.12	2.735	1.683	179.9	
	N2···HN4	0.111	0.000	5.10	2.594	1.412	179.0	
Key point 11 (6.05 Bohr): $G^{*}_{N2}\cdot C$(rWC)	O6H···O2	0.047	0.134	3.32	2.666	1.670	172.7	7.15
	N1H···N3	0.042	0.101	6.53	2.851	1.815	179.0	
	N2···HN4	0.048	0.094	7.08	2.816	1.756	176.4	

*For footnote definitions see **Table 3**.*

III. G*·C*(rWC)↔$G^{*\prime}_{N2}$·C(rWC), IV. G*′·C*(H)↔G^{*}_{N7}·C(H) and V. G*′·C*(rH)↔$G^{*\prime}_{N7}$·C(rH) reactions (**Figures 2**, **4**, **6**, **8**, **10**, **Tables 3**–**7**).

We have established following regularities of the general character for the obtained sweeps of the most important physico-chemical parameters along the IRC.

The widths of the reaction zone of the investigated reactions starting from the reagent and till the product are almost the same for the I. G*·C*(rWC)↔G·C^{*}_{O2}(rWC) (9.24); II. G*·C*(rWC)↔G^{*}_{N2}·C(rWC) (10.54) and IV. G*′·C*(H)↔G^{*}_{N7}·C(H) (9.30 Bohr), while these widths are significantly larger for the III. G*·C*(rWC)↔$G^{*\prime}_{N2}$·C(rWC) (14.49) and V. G*′·C*(rH)↔$G^{*\prime}_{N7}$·C(rH) (23.12 Bohr) reactions (**Figures 2**, **4**, **6**, **8**, **10**).

All tautomerisation processes are dipole-active, since they are followed by the significant change of the dipole moment μ of the tautomerising base pair (**Figures 3C**, **5C**, **7C**, **9C**, **11C**). These dependencies are U-like with maximal and minimal values located in the transition state zone for the I. G*·C*(rWC)↔G·C^{*}_{O2}(rWC) SPT (values of μ change in the range: 3.15–6.54); II. G*·C*(rWC)↔G^{*}_{N2}·C(rWC) SPT (3.15–7.15); III. G*·C*(rWC)↔$G^{*\prime}_{N2}$·C(rWC) DPT

TABLE 5 | Electron-topological and structural characteristics of the specific intermolecular bonds revealed in the 9 key points and the polarity of the latters along the IRC of the III. G*·C*(rWC)↔G*′$_{N2}$·C(rWC) tautomerisation obtained at the B3LYP/6-311++G(d,p) level of theory in vacuum (see **Figure 6**).

Complex	AH· · · B H-bond/ A-H/H-B covalent bond	ρ^a	$\Delta\rho^b$	$100 \cdot \varepsilon^c$	$d^d_{A\cdots B}$	$d^e_{H\cdots B}$	$\angle_{AH\cdots B}{}^f$	μ^g
Key point 1 (−10.37 Bohr): G*·C*(rWC)	O6H···O2	0.038	0.124	3.31	2.731	1.753	171.1	6.54
	N1···HN3	0.035	0.086	6.32	2.932	1.894	173.6	
	N2H···N4	0.026	0.077	8.04	3.036	2.016	178.0	
Key point 2 (−3.23 Bohr): $\Delta\rho_{N1\cdots H} = 0$	O6H···O2	0.055	0.147	3.48	2.608	1.612	169.8	4.99
	N1···HN3	0.115	−0.010	4.65	2.602	1.404	173.1	
	N2···N4	0.018	0.065	65.91	2.818	–	–	
Key point 3 (−3.02 Bohr): $\rho_{N1-H} = \rho_{H-N3}$	O6H···O2	0.057	0.144	3.48	2.607	1.604	170.3	4.17
	N1-H/H-N3	0.150	−0.187	4.06	2.603	1.303	172.4	
	N2H···N4	0.019	0.066	53.46	2.815	2.293	110.5	
Key point 4 (−2.61 Bohr): $\Delta\rho_{H\cdots N3} = 0$	O6H···O2	0.058	0.139	3.50	2.607	1.594	171.0	3.31
	N1H···N3	0.107	0.002	5.19	2.617	1.445	169.8	
	N2H···N4	0.022	0.075	21.37	2.801	2.169	118.3	
Key point 5 (−0.21 Bohr): $\Delta\rho_{H\cdots N4} = 0$	O6H···O2	0.050	0.129	3.84	2.662	1.657	170.8	3.53
	N1H···N3	0.061	0.100	7.18	2.691	1.670	158.7	
	N2H···N4	0.111	0.007	3.50	2.576	1.418	163.2	
Key point 6 (0.00 Bohr): $TS_{G^*\cdot C^*(rWC)\leftrightarrow G^{*\prime}N2\cdot C(WC)}$	O6H···O2	0.049	0.131	3.84	2.663	1.662	170.6	4.55
	N1H···N3	0.059	0.105	7.29	2.692	1.682	158.2	
	N2-HN4	0.155	−0.214	3.17	2.575	1.287	164.5	
	N2H-N4	0.147	−0.161	3.53	2.575	1.312	164.5	
Key point 7 (0.02 Bohr): $\rho_{N2-H} = \rho_{H-N4}$	O6H···O2	0.049	0.131	3.80	2.664	1.663	170.6	4.85
	N1H···N3	0.058	0.106	7.30	2.693	1.684	158.1	
	N2-H/H-N4	0.157	−0.225	3.50	2.575	1.286	164.7	
Key point 8 (0.26 Bohr): $\Delta\rho_{N2\cdots H} = 0$	O6H···O2	0.048	0.133	3.83	2.665	1.668	170.4	6.05
	N1H···N3	0.057	0.111	7.40	2.694	1.694	157.7	
	N2···HN4	0.108	0.005	3.21	2.580	1.419	165.0	
Key point 9 (4.12 Bohr): $G^{*\prime}_{N2}$·C(rWC)	O6H···O2	0.037	0.117	3.87	2.750	1.768	170.4	8.85
	N1H···N3	0.033	0.095	8.50	2.876	1.921	153.8	
	N2···HN4	0.024	0.071	11.36	3.014	2.023	160.2	

*For footnote definitions see **Table 3**.*

(2.81–8.84) and V. G*′·C*(rH)↔G*′$_{N7}$·C(rH) DPT (4.47–9.01 D) reactions, while it is reverse with maximal values at the transition state zone for the IV. G*′·C*(H)↔G^*_{N7}·C(H) reaction (5.16–10.12 D) DPT (**Figures 3C**, **5C**, **7C**, **9C**, **11C**).

Tautomerisation process does not change the configuration of the base pair—complexes slightly compress on several dozens of Angstrom at the zone of the TSs of tautomerisation. TSs demonstrate significant deviations from a plane in the case, when steric conflicts arise between the interacting exocyclic groups (**Figures 2**, **4**, **6**, **8**, **10**).

According to the authors' conception (Brovarets' and Hovorun, 2013a,b,c,d, 2014c,d, 2015h,i; Brovarets' et al., 2013a,b, 2014a,b,c, 2015), it was introduced key points, namely 11 key points were obtained in the cases of the I. G*·C*(rWC)↔G·C^*_{O2}(rWC) and II. G*·C*(rWC)↔G^*_{N2}·C(rWC) SPT along the IRC in contrast to the processes of the III. G*·C*(rWC)↔G*′$_{N2}$·C(rWC), IV. G*′·C*(H)↔G^*_{N7}·C(H) and V. G*′·C*(rH)↔G*′$_{N7}$·C(rH) DPT, for which 9 key points have been localized.

At this, it was obtained typical crossings of the profiles for the electron density ρ, the Laplacian of the electron density Δρ and the distance $d_{AH/HB}$ between the hydrogen and electronegative A or B atoms for the H-bonds involved in the tautomerisation, notifying the equalization of these parameters. They occur at the 3rd and 9th key points in the case of the reaction I, 3rd and 8th—for the reaction II, 3rd and 7th—for the reactions III and IV and 3rd and 6th—for the reaction V (**Figures 3G,H,K**, **5G,H,K**, **7G,H,K**, **9G,H,K**, **11G,H,K**).

One and the same regularity is observed for the dE/dIRC function in all cases of tautomerisations—with two local maxima and two local minima achieved at the TS zone (**Figures 3B**, **5B**, **7B**, **9B**, **11B**).

Also it was observed five patterns for the energy E_{HB} of the intermolecular H-bonds, estimated by the EML method (Espinosa et al., 1998; Matta et al., 2006b; Mata

TABLE 6 | Electron-topological and structural characteristics of the specific intermolecular bonds revealed in the 9 key points and the polarity of the latters along the IRC of the IV. $G^{*\prime}\cdot C^{*}(H)\leftrightarrow G^{*}_{N7}\cdot C(H)$ tautomerisation obtained at the B3LYP/6-311++G(d,p) level of theory in vacuum (see **Figure 8**).

Complex	AH· · ·B H-bond/ A-H/H-B covalent bond	ρ^a	$\Delta\rho^b$	$100\cdot\varepsilon^c$	$d^d_{A\cdots B}$	$d^e_{H\cdots B}$	$\angle_{AH\cdots B}{}^f$	μ^g
Key point 1 (−6.04 Bohr): $G^{*\prime}\cdot C^{*}(H)$	O6H···N4	0.047	0.102	4.88	2.710	1.742	160.7	5.16
	N7···HN3	0.032	0.101	5.68	2.834	1.791	180.0	
	C8H···O2	0.003	0.012	1.73	3.675	3.029	118.9	
Key point 2 (−1.17 Bohr): $\Delta\rho_{O6\cdots H}=0$	O6H···N4	0.113	0.007	3.73	2.484	1.397	164.9	6.89
	N7···HN3	0.077	0.098	4.56	2.634	1.558	175.4	
	C8H···O2	0.006	0.022	15.15	3.344	2.716	116.8	
Key point 3 (−0.96 Bohr): $\rho_{O6-H}=\rho_{H-N4}$	O6-H/H-N4	0.165	−0.262	1.52	2.428	1.214	166.3	8.27
	N7···HN3	0.080	0.089	4.45	2.631	1.544	175.6	
	C8H···O2	0.006	0.022	15.27	3.343	2.716	116.7	
Key point 4 (−0.74 Bohr): $\Delta\rho_{H\cdots N4}=0$	O6···HN4	0.126	0.023	1.77	2.494	1.313	166.6	9.45
	N7···HN3	0.085	0.076	4.30	2.626	1.523	175.7	
	C8H···O2	0.006	0.022	14.99	3.338	2.710	116.8	
Key point 5 (−0.10 Bohr): $\Delta\rho_{N7\cdots H}=0$	O6···HN4	0.091	0.136	2.15	2.534	1.432	167.7	9.96
	N7···HN3	0.111	0.004	3.72	2.589	1.420	175.7	
	C8H···O2	0.007	0.024	12.56	3.305	2.668	117.3	
Key point 6 (0.00 Bohr): $TS_{G^{*\prime}\cdot C^{*}(H)\leftrightarrow G^{*}N7\cdot C(H)}$	O6···HN4	0.088	0.143	2.19	2.539	1.446	167.7	9.63
	N7-HN3	0.124	−0.053	3.48	2.583	1.374	176.0	
	N7H-N3	0.191	−0.493	3.58	2.583	1.210	176.0	
	C8H···O2	0.007	0.024	12.24	3.303	2.665	117.4	
Key point 7 (0.17 Bohr): $\rho_{N7-H}=\rho_{H-N3}$	O6···HN4	0.084	0.152	2.23	2.543	1.463	167.7	8.84
	N7-H/H-N3	0.156	−0.231	3.09	2.580	1.288	176.2	
	C8H···O2	0.007	0.024	11.61	3.302	2.662	117.5	
Key point 8 (0.41 Bohr): $\Delta\rho_{H\cdots N3}=0$	O6···HN4	0.079	0.161	2.28	2.548	1.482	167.6	7.73
	N7H···N3	0.112	0.006	4.55	2.583	1.414	176.3	
	C8H···O2	0.007	0.024	10.78	3.301	2.657	117.8	
Key point 9 (3.26 Bohr): $G^{*}_{N7}\cdot C(H)$	O6···HN4	0.045	0.137	2.53	2.728	1.689	172.2	7.32
	N7H···N3	0.054	0.099	5.95	2.758	1.700	177.2	
	C8H···O2	0.006	0.022	16.54	3.324	2.711	115.8	

*For footnote definitions see **Table 3**.*

et al., 2011; Lecomte et al., 2015; Alkorta et al., 2016, 2017), along the IRC for the I, II, IV and V reactions and four patterns—for the III reaction (**Figure 12**, **Table 8**). These sweeps allow to estimate numerically the cooperativity of the neighboring H-bonds according to the methodology, proposed by us earlier (Brovarets' and Hovorun, 2019b). It was established the general pattern—the anti-parallel H-bonds amplify each other and parallel—weaken each other (Turaeva and Brown-Kennerly, 2015). Moreover, some of the dependencies of the energy E_{HB} of the intermolecular H-bonds exist during entire IRC, such as (G)N2H…N4(C) for the I. $G^{*}\cdot C^{*}(rWC)\leftrightarrow G\cdot C^{*}_{O2}(rWC)$ reaction, (G)O6H…O2(C) for the II. $G^{*}\cdot C^{*}(rWC)\leftrightarrow G^{*}_{N2}\cdot C(rWC)$ reaction, (G)O6H…O2(C) for the III. $G^{*}\cdot C^{*}(rWC)\leftrightarrow G^{*\prime}{}_{N2}\cdot C(rw_{WC})$ reaction, (G)C8H…O2(C) (its energy remains almost unchangeable during the IRC) for the $G^{*\prime}\cdot C^{*}(H)\leftrightarrow G^{*}_{N7}\cdot C(H)$ reaction and (G)O6H…O2(C) for the $G^{*\prime}\cdot C^{*}(rH)\leftrightarrow G^{*\prime}{}_{N7}\cdot C(rH)$ reaction. In the case of the III. $G^{*}\cdot C^{*}(rWC)\leftrightarrow G^{*\prime}{}_{N2}\cdot C(rw_{WC})$ reaction, some of the H-bonds transform into the van der Waals contact and then to another H-bonds during the IRC: (G)N2H…N4(C) H-bond → (G)N2…N4(C) vdW contact → (G)N2H…N4(C) H-bond for the III. $G^{*}\cdot C^{*}(rWC)\leftrightarrow G^{*\prime}{}_{N2}\cdot C(rw_{WC})$ reaction (**Figure 12**). For more details according the patterns refer to **Table 8**.

Finally, we would like to note some general regularities, which are characteristic for all without exclusion processes of tautomerisation.

Thus, in the vast majority of cases base pairs are plane symmetric structures during the entire PT and DPT tautomerization processes along the IRC, despite the ability of the DNA bases for the out-of-plane bending (Govorun et al., 1992; Hovorun et al., 1999; Nikolaienko et al., 2011), excluding two mentioned above cases, when there are deviation from the planarity—III. $G^{*}\cdot C^{*}(rWC)\leftrightarrow G^{*\prime}{}_{N2}\cdot C(rWC)$ (**Figure 1**).

TABLE 7 | Electron-topological and structural characteristics of the specific intermolecular bonds revealed in the 9 key points and the polarity of the latters along the IRC of the V. G*′·C*(rH)↔G*′$_{N7}$·C(rH) tautomerisation obtained at the B3LYP/6-311++G(d,p) level of theory in vacuum (see **Figure 10**).

Complex	AH· · ·B H-bond/ A-H/H-B covalent bond	ρ^a	$\Delta\rho^b$	$100\cdot\varepsilon^c$	$dA\cdot\cdot\cdot B^d$	$dH\cdot\cdot\cdot B^e$	$\angle_{AH\cdots B}{}^f$	μ^g
Key point 1 (−13.94 Bohr): G*′·C*(rH)	O6H···O2	0.034	0.120	2.25	2.733	1.785	160.6	5.43
	N7···HN3	0.042	0.101	2.73	2.838	1.797	176.3	
	C8H···N4	0.004	0.013	3.58	3.681	3.015	120.4	
Key point 2 (−1.33 Bohr): $\Delta\rho_{N7\cdots H}=0$	O6H···O2	0.009	0.027	2.75	3.365	2.407	167.6	5.11
	N7···HN3	0.121	−0.007	3.60	2.545	1.377	167.2	
	C8H···N4	0.044	0.124	3.78	2.740	1.814	139.8	
Key point 3 (−1.12 Bohr): $\rho_{N67-H}=\rho_{H-N3}$	O6H···O2	0.009	0.027	2.82	3.366	2.406	167.9	4.70
	N7-H/H-N3	0.161	−0.256	4.13	2.549	1.283	166.5	
	C8H···N4	0.047	0.124	4.09	2.730	1.783	141.6	
Key point 4 (−0.71 Bohr): $\Delta\rho_{H\cdots N3}=0$	O6H···O2	0.009	0.027	2.77	3.367	2.405	168.1	4.47
	N7H···N3	0.110	0.003	4.75	2.564	1.430	163.8	
	C8H···N4	0.061	0.116	4.87	2.700	1.668	148.7	
Key point 5 (−0.20 Bohr): $\Delta\rho_{H\cdots N4}=0$	O6H···O2	0.009	0.027	2.67	3.368	2.408	167.9	4.93
	N7H···N3	0.090	0.073	5.10	2.574	1.506	161.6	
	C8H···N4	0.111	−0.010	4.53	2.679	1.425	157.2	
Key point 6 (−0.04 Bohr): $\rho_{C8-H}=\rho_{H-N4}$	O6H···O2	0.009	0.027	2.66	3.368	2.409	167.9	5.38
	N7H···N3	0.087	0.084	5.16	2.576	1.520	161.2	
	C8-H/H-N4	0.137	−0.202	2.32	2.677	1.341	158.5	
Key point 7 (0.00 Bohr): $TS_{G^{*\prime}\cdot C^*(rH)\leftrightarrow G^{*\prime}N7\cdot C(rH)}$	O6H···O2	0.009	0.027	2.66	3.368	2.409	167.9	5.51
	N7H···N3	0.086	0.087	5.18	2.576	1.524	161.1	
	C8-HN4	0.131	−0.174	2.36	2.677	1.320	158.8	
	C8H-N4	0.145	−0.169	4.22	2.677	1.404	158.8	
Key point 8 (0.36 Bohr): $\Delta\rho_{C8\cdots H}=0$	O6H···O2	0.009	0.027	2.62	3.369	2.411	167.7	6.81
	N7H···N3	0.079	0.107	5.31	2.581	1.554	160.0	
	$C8^-\cdots$HN4	0.084	0.003	3.08	2.681	1.581	160.7	
Key point 9 (9.18 Bohr): G*′$_{N7}$·C(rH)	O6H···O2	0.022	0.080	3.15	2.918	1.968	162.9	9.01
	N7H···N3	0.049	0.114	6.60	2.758	1.743	167.8	
	$C8^-\cdots$HN4	0.016	0.038	6.19	3.302	2.316	160.1	

For footnote definitions see ***Table 3****.*

Interestingly, the total energy of the intermolecular H-bonds only partially contributes to the electron energy of the monomers interactions among all without any exceptions H-bonded structures investigated in this work (see **Figures 1**, **12**). This result is in a good accordance with generalized literature data (Brovarets' and Hovorun, 2014e, 2019b).

CONCLUSIONS

For the first time the tautomerisation of the biologically-important conformers of the G*·C* DNA base pair - reverse Löwdin G*·C*(rWC), Hoogsteen G*′·C*(H) and reverse Hoogsteen G*′·C*(rH) pairs - was investigated and thoroughly analyzed. It was found out that the G*·C*(rWC)↔$G^+\cdot C^-$(rWC)↔G·C^*_{O2}(rWC) and G*·C*(rWC)↔$G^+\cdot C^-$(rWC)↔G^*_{N2}·C(rWC) tautomerization processes occur *via* the two-stage sequential SPT *via* dynamically-unstable zwitterion-like $G^+\cdot C^-$(rWC) intermediate, while the G*·C*(rWC)↔G*′$_{N2}$·C(rw_{WC}), G*′·C*(H)↔G^*_{N7}·C(H), and G*′·C*(rH)↔G*′$_{N7}$·C(rH) tautomerization processes occur through the one-stage DPT. At this, proton transfer along the non-canonical (G*)CH…N(C*) H-bond is accompanied by the significant deviation of the C-H-N bridge at the TS.

Obtained data evidence that among the G*·C*(rWC), G′·C*(H) and G*′ · C*(rH) base pairs only the tautomerisation of the latest of them lead to the formation of the dynamically stable G*′$_{N7}$·C(rH) base pair with lifetime 5.15 ps with a miserable population $2.3\cdot10^{-17}$.

Moreover, it was revealed that the I. G*·C*(rWC)↔$G^+\cdot C^-$(rWC)↔G·C^*_{O2}(rWC) and II. G*·C*(rWC)↔$G^+\cdot C^-$(rWC)↔G^*_{N2}·C(rWC) tautomerization reactions proceed in *a synchronous concerted manner via the stepwise SPT*, while the III. G*·C*(rWC)↔G*′$_{N2}$·C(rWC), IV. G*′·C*(H)↔G^*_{N7}·C(H), and V. G*′·C*(rH)↔G*′$_{N7}$·C(rH) reactions occur in *an asynchronous concerted manner via the DPT*.

TABLE 8 | Patterns of the specific intermolecular interactions including AH···B H-bonds and loosened A-H-B covalent bridges that sequentially replace each other along the IRC of the investigated tautomerisations *via* the SPT or DPT obtained at the B3LYP/6-311++G(d,p) level of theory (see **Figure 12**).

Patterns	IRC range, Bohr	Specific intermolecular interactions, forming patterns
I. G*·C*(rWC)↔G^{+}·C^{-}(rWC)↔G·C^{*}_{O2}(rWC)		
I	[−4.49 ÷ −0.27)	(G)O6H···O2(C), (G)N1···HN3(C), (G)N2H···N4(C)
II	[−0.27 ÷ 0.12)	(G)O6H···O2(C), (G)N1-H/H-N3(C), (G)N2H···N4(C)
III	[0.12 ÷ 2.13)	(G)O6H···O2(C), (G)N1H···N3(C), (G)N2H···N4(C)
IV	[2.13 ÷ 2.51)	(G)O6-H/H-O2(C), (G)N1H···N3(C), (G)N2H···N4(C)
V	[2.51 ÷ 4.75]	(G)O6···HO2(C), (G)N1H···N3(C), (G)N2H···N4(C)
II. G*·C*(rWC)↔G^{+}·C^{-}(rWC)↔G^{*}_{N2}·C(rWC)		
I	[−4.49÷ − 0.27)	(G)O6H···O2(C), (G)N1···HN3(C), (G)N2H···N4(C)
II	[−0.27 ÷ 0.12)	(G)O6H···O2(C), (G)N1-H/H-N3(C), (G)N2H···N4(C)
III	[0.12 ÷ 4.52)	(G)O6H···O2(C), (G)N1H···N3(C), (G)N2H···N4(C)
IV	[4.52 ÷ 4.91)	(G)O6H···O2(C), (G)N1H···N3(C), (G)N2-H/H-N4(C)
V	[4.91 ÷ 6.05]	(G)O6H···O2(C), (G)N1H···N3(C), (G)N2···HN4(C)
III. G*·C*(rWC)↔$G^{*\prime}_{N2}$·C(rw_{WC})		
I	[−10.37 ÷ −4.79)	(G)O6H···O2(C), (G)N1···HN3(C), (G)N2H···N4(C)
II	[−4.79 ÷ −3.23)	(G)O6H···O2(C), (G)N1···HN3(C), (G)N2···N4(C)
III	[−3.23 ÷ −2.71)	(G)O6H···O2(C), (G)N1-H/H-N3(C), (G)N2H···N4(C)
IV	[−2.71 ÷ −0.16)	(G)O6H···O2(C), (G)N1H···N3(C), (G)N2H···N4(C)
V	[−0.16 ÷ 0.21)	(G)O6H···O2(C), (G)N1H···N3(C), (G)N2-H/H-N4(C)
VI	[0.21 ÷ 4.12]	(G)O6H···O2(C), (G)N1H···N3(C), (G)N2···HN4(C)
IV. $G^{*\prime}$·C*(H)↔G^{*}_{N7}·C(H)		
I	[−6.04 ÷ −1.17)	(G)O6H···N4(C), (G)N7···HN3(C), (G)C8H···O2(C)
II	[−1.17 ÷ −0.74)	(G)O6-H/H-N4(C), (G)N7···HN3(C), (G)C8H···O2(C)
III	[−0.74 ÷ −0.10)	(G)O6···HN4(C), (G)N7···HN3(C), (G)C8H···O2(C)
IV	[−0.10 ÷ 0.37)	(G)O6···HN4(C), (G)N7-H/H-N3(C), (G)C8H···O2(C)
V	[0.37 ÷ 3.26]	(G)O6···HN4(C), (G)N7H···N3(C), (G)C8H···O2(C)
V. $G^{*\prime}$·C*(rH)↔$G^{*\prime}_{N7}$·C(rH)		
I	[−13.94 ÷ −1.33)	(G)O6H···O2(C), (G)N7···HN3(C), (G)C8H···N4(C)
II	[−1.33 ÷ −0.71)	(G)O6H···O2(C), (G)N7-H/H-N3(C), (G)C8H···N4(C)
III	[−0.71 ÷ −0.20)	(G)O6H···O2(C), (G)N7H···N3(C), (G)C8H···N4(C)
IV	[−0.20 ÷ 0.31)	(G)O6H···O2(C), (G)N7H···N3(C), (G)C8-H/H-N4(C)
V	[0.31 ÷ 9.18]	(G)O6H···O2(C), (G)N7H···N3(C), (G)C8···HN4(C)

We have also established dependencies of the most important physico-chemical parameters along the IRC enabling to understand more precisely the inherent nature of the investigated processes.

DATA AVAILABILITY

The datasets generated for this study are available on request to the corresponding author.

AUTHOR CONTRIBUTIONS

OB analysis and preparation of the current literature survey, discussion of the strategy of the current investigation, study conception and design, acquisition of data, drafting of manuscript analysis and interpretation of data, performance of calculations, discussion of the obtained data, preparation of the numerical data for **Tables 1–8**, graphical materials for **Figures 1–12**, and text of the manuscript. TO preparation of the numerical data for **Tables 1–8** and graphical materials for **Figures 1–12**. DH study conception, critical revision of manuscript, proposition of the task of the investigation, discussion of the obtained data, and preparation of the text of the manuscript. All authors were involved in the proofreading of the final version of the manuscript.

ACKNOWLEDGMENTS

Authors sincerely grateful for technical support to Dr. Ivan Voiteshenko (Taras Shevchenko National University of Kyiv) and computational facilities of joint computer cluster of SSI Institute for Single Crystals of the National Academy of Sciences of Ukraine (NASU) and Institute for Scintillation Materials

of the NASU incorporated into Ukrainian National Grid. DrSci OB expresses sincere gratitude to the U.S.-Ukraine Foundation (USUF) Biotech Initiative for a travel grant (2018 Emerging Biotech Leader of Ukraine; https://www.usukraine.org/biotechnology-initiative/), enabling to participate in the 63rd Annual Meeting of the Biophysical Society BPS'2019 (Baltimore, Maryland, March 2–6, 2019; https://www.biophysics.org/2019meeting#/; https://bioukraine.org/news/emerging-biotech-leader-olha-brovarets-attends-63rd-biophysical-society-meeting-in-baltimore/; https://bioukraine.org/news/emerging-leader-olha-brovarets-shares-her-us-experience-with-bionity-student-biotech-club/).

REFERENCES

Acosta-Reyes, F. J., Alechaga, E., Subirana, J. A., and Campos, J. L. (2015). Structure of the DNA duplex d(ATTAAT)$_2$ with Hoogsteen hydrogen bonds. *PLoS ONE* 10:e0120241. doi: 10.1371/journal.pone.0120241

Al-Khalili, J., and McFadden, J. (2014). *Life on the Edge: the Coming of Age of Quantum Biology*. London: Bantam Press.

Alkorta, I., Mata, I., Molins, E., and Espinosa, E. (2016). Charged versus neutral hydrogen-bonded complexes: is there a difference in the nature of the hydrogen bonds? *Chem. Eur. J.* 22, 9226–9234. doi: 10.1002/chem.201600788

Alkorta, I., Mata, I., Molins, E., and Espinose, E. (2018). Energetic, topological and electric field analyses of cation-cation nucleic acid interactions in Watson-Crick disposition. *ChemPhysChem* 20, 148–158. doi: 10.1002/cphc.201800878

Alkorta, I., Thacker, J. C. R., and Popelier, P. L. A. (2017). An interacting quantum atom study of model S_N2 reactions (X–··CH_3X, X = F, Cl, Br, and I). *J. Comput. Chem.* 39, 546–556. doi: 10.1002/jcc.25098

Alvey, H. S., Gottardo, F. L., Nikolova, E. N., and Al-Hashimi, H. M. (2014). Widespread transient Hoogsteen base-pairs in canonical duplex DNA with variable energetics. *Nat. Comm.* 5, 4786–4794. doi: 10.1038/ncomms5786

Arabi, A., and Matta, C. F. (2018). Adenine–thymine tautomerization under the influence of strong homogeneous electric fields. *Phys. Chem. Chem. Phys.* 20, 12406–12412. doi: 10.1039/C8CP01122B

Atkins, P. W. (1998). *Physical Chemistry*. Oxford: Oxford University Press.

Bader, R. F. W. (1990). *Atoms in Molecules: A Quantum Theory*. Oxford: Oxford University Press.

Bertran, J., Blancafort, L., Noguera, M., and Sodupe, M. (2006). "Proton transfer in DNA base pairs," in *Computational Studies of RNA and DNA*, eds J. Šponer and F. Lankaš (Dordrecht: Springer), 411–432. doi: 10.1007/978-1-4020-4851-3_16

Boutis, T. (1992). *Proton Transfer in Hydrogen Bonded Systems*. New York, NY: Plenum. doi: 10.1007/978-1-4615-3444-0

Boys, S. F., and Bernardi, F. (1970). The calculation of small molecular interactions by the differences of separate total energies. Some procedures with reduced errors. *Mol. Phys.* 19, 553–566. doi: 10.1080/00268977000101561

Brovarets', O. O. (2013a). Structural and energetic properties of the four configurations of the A·T and G·C DNA base pairs. *Ukr. Biochem. J.* 85, 104–110. doi: 10.15407/ubj85.04.104

Brovarets', O. O. (2013b). Under what conditions does G·C Watson-Crick DNA base pair acquire all four configurations characteristic for A·T Watson-Crick DNA base pair? *Ukr. Biochem. J.* 85, 98–103. doi: 10.15407/ubj85.04.098

Brovarets', O. O., and Hovorun, D. M. (2009). Physicochemical mechanism of the wobble DNA base pairs Gua·Thy and Ade·Cyt transition into the mismatched base pairs Gua*·Thy and Ade·Cyt* formed by the mutagenic tautomers. *Ukr. Bioorg. Acta.* 8, 12–18.

Brovarets', O. O., and Hovorun, D. M. (2010). Quantum-chemical investigation of tautomerization ways of Watson-Crick DNA base pair guanine-cytosine. *Ukr. Biochem. J.* 82, 55–60.

Brovarets', O. O., and Hovorun, D. M. (2013a). Atomistic understanding of the C·T mismatched DNA base pair tautomerization *via* the DPT: QM and QTAIM computational approaches. *J. Comput. Chem.* 34, 2577–2590. doi: 10.1002/jcc.23412

Brovarets', O. O., and Hovorun, D. M. (2013b). Atomistic nature of the DPT tautomerisation of the biologically important C·C* DNA base mispair containing amino and imino tautomers of cytosine: a QM and QTAIM approach. *Phys. Chem. Chem. Phys.* 15, 20091–20104. doi: 10.1039/c3cp52644e

Brovarets', O. O., and Hovorun, D. M. (2013c). Prototropic tautomerism and basic molecular principles of hypoxanthine mutagenicity: an exhaustive quantum-chemical analysis. *J. Biomol. Struct. Dynam.* 31, 913–936. doi: 10.1080/07391102.2012.715041

Brovarets', O. O., and Hovorun, D. M. (2013d). DPT tautomerization of the long A·A* Watson-Crick base pair formed by the amino and imino tautomers of adenine: combined QM and QTAIM investigation. *J. Mol. Model.* 19, 4223–4237. doi: 10.1007/s00894-013-1880-2

Brovarets', O. O., and Hovorun, D. M. (2014a). Why the tautomerization of the G·C Watson–Crick base pair *via* the DPT does not cause point mutations during DNA replication? QM and QTAIM comprehensive analysis. *J. Biomol. Struct. Dynam.* 32, 1474–1499. doi: 10.1080/07391102.2013.822829

Brovarets', O. O., and Hovorun, D. M. (2014b). Can tautomerisation of the A·T Watson-Crick base pair *via* double proton transfer provoke point mutations during DNA replication? A comprehensive QM and QTAIM analysis. *J. Biomol. Struct. Dynam.* 32, 127–154. doi: 10.1080/07391102.2012.755795

Brovarets', O. O., and Hovorun, D. M. (2014c). How the long G·G* Watson-Crick DNA base mispair comprising keto and enol tautomers of the guanine tautomerises? The results of the QM/QTAIM investigation. *Phys. Chem. Chem. Phys.* 6, 15886–15899. doi: 10.1039/C4CP01241K

Brovarets', O. O., and Hovorun, D. M. (2014d). DPT tautomerisation of the G·A_{syn} and A*·G^*_{syn} DNA mismatches: A QM/QTAIM combined atomistic investigation. *Phys. Chem. Chem. Phys.* 16, 9074–9085. doi: 10.1039/C4CP00488D

Brovarets', O. O., and Hovorun, D. M. (2014e). Does the G·G^*_{syn} DNA mismatch containing canonical and rare tautomers of the guanine tautomerise through the DPT? *A* QM/QTAIM microstructural study. *Mol. Phys.* 112, 3033–3046. doi: 10.1080/00268976.2014.927079

Brovarets', O. O., and Hovorun, D. M. (2015a). Wobble↔Watson-Crick tautomeric transitions in the homo-purine DNA mismatches: a key to the intimate mechanisms of the spontaneous transversions. *J. Biomol. Struct. Dynam.* 33, 2710–2715. doi: 10.1080/07391102.2015.1077737

Brovarets', O. O., and Hovorun, D. M. (2015b). Novel physico-chemical mechanism of the mutagenic tautomerisation of the Watson–Crick-like A·G and C·T DNA base mispairs: a quantum-chemical picture. *RSC Adv.* 5, 66318–66333. doi: 10.1039/C5RA11773A

Brovarets', O. O., and Hovorun, D. M. (2015c). A novel conception for spontaneous transversions caused by homo-pyrimidine DNA mismatches: a QM/QTAIM highlight. *Phys. Chem. Chem. Phys.* 17, 21381–21388. doi: 10.1039/C5CP03211C

Brovarets', O. O., and Hovorun, D. M. (2015d). Tautomeric transition between wobble A·C DNA base mispair and Watson-Crick-like A·C* mismatch: miscrostructural mechanism and biological significance. *Phys. Chem. Chem. Phys.* 17, 15103–15110. doi: 10.1039/C5CP01568E

Brovarets', O. O., and Hovorun, D. M. (2015e). How many tautomerisation pathways connect Watson-Crick-like G*·T DNA base mispair and wobble mismatches? *J. Biomol. Struct. Dynam.* 33, 2297–2315. doi: 10.1080/07391102.2015.1046936

Brovarets', O. O., and Hovorun, D. M. (2015f). New structural hypostases of the A·T and G·C Watson-Crick DNA base pairs caused by their mutagenic tautomerisation in a wobble manner: a QM/QTAIM prediction. *RSC Adv.* 5, 99594–99605. doi: 10.1039/C5RA19971A

Brovarets', O. O., and Hovorun, D. M. (2015g). Proton tunneling in the A·T Watson-Crick DNA base pair: myth or reality? *J. Biomol. Struct. Dynam.* 12, 2716–2720. doi: 10.1080/07391102.2015.1092886

Brovarets', O. O., and Hovorun, D. M. (2015h). The physicochemical essence of the purine·pyrimidine transition mismatches with Watson-Crick geometry in DNA: A·C* *versa* A*·C. A QM and QTAIM atomistic understanding. *J. Biomol. Struct. Dynam.* 33, 28–55. doi: 10.1080/07391102.2013.852133

Brovarets', O. O., and Hovorun, D. M. (2015i). The nature of the transition mismatches with Watson-Crick architecture: the G*·T or G·T* DNA base

mispair or both? A QM/QTAIM perspective for the biological problem. *J. Biomol. Struct. Dynam*. 33, 925–945. doi: 10.1080/07391102.2014.924879

Brovarets', O. O., and Hovorun, D. M. (2016). By how many tautomerisation routes the Watson-Crick-like A·C* DNA base mispair is linked with the wobble mismatches? A QM/QTAIM vision from a biological point of view. *Struct. Chem*. 27, 119–131. doi: 10.1007/s11224-015-0687-4

Brovarets', O. O., and Hovorun, D. M. (2018). "Renaissance of the tautomeric hypothesis of the spontaneous point mutations in DNA: new ideas and computational approaches," in *Mitochondrial DNA - New Insights*, ed H. Seligmann (London: IntechOpen), 31–55.

Brovarets', O. O., and Hovorun, D. M. (2019a). Key microstructural mechanisms of the 2-aminopurine mutagenicity: results of extensive quantum-chemical research. *J. Biomol. Struct. Dyn*. 37, 2716–2732. doi: 10.1080/07391102.2018.1495577

Brovarets', O. O., and Hovorun, D. M. (2019b). Atomistic mechanisms of the double proton transfer in the H-bonded nucleobase pairs: QM/QTAIM computational lessons. *J. Biomol. Struct. Dyn*. 37, 1880–1907. doi: 10.1080/07391102.2018.1467795

Brovarets', O. O., and Pérez-Sánchez, H. E. (2016). Whether the amino-imino tautomerism of 2-aminopurine is involved into its mutagenicity? Results of a thorough QM investigation. *RSC Adv*. 110, 108255–108264. doi: 10.1039/C6RA24277D

Brovarets', O. O., and Pérez-Sánchez, H. E. (2017). Whether 2-aminopurine induces incorporation errors at the DNA replication? A quantum-mechanical answer on the actual biological issue. *J. Biomol. Struct. Dynam*. 35, 3398–3411. doi: 10.1080/07391102.2016.1253504

Brovarets', O. O., Pérez-Sánchez, H. E., and Hovorun, D. M. (2016). Structural grounds for the 2-aminopurine mutagenicity: a novel insight into the old problem of the replication errors. *RSC Adv*. 6, 99546–99557. doi: 10.1039/C6RA17787E

Brovarets', O. O., and Tsiupa, K. S. (2019). Novel conformationally-tautomeric properties of the biologically important A·T DNA base pairs. *Biophys. J.* 116:75a. doi: 10.1016/j.bpj.2018.11.446

Brovarets', O. O., Tsiupa, K. S., Dinets, A., and Hovorun, D. M. (2018d). Unexpected routes of the mutagenic tautomerization of the T nucleobase in the classical A·T DNA base pairs: a QM/QTAIM comprehensive view. *Front. Chem*. 6:532. doi: 10.3389/fchem.2018.00532

Brovarets', O. O., Tsiupa, K. S., and Hovorun, D. M. (2018a). Non-dissociative structural transitions of the Watson-Crick and reverse Watson-Crick A·T DNA base pairs into the Hoogsteen and reverse Hoogsteen forms. *Sci. Repts*. 8:10371. doi: 10.1038/s41598-018-28636-y

Brovarets', O. O., Tsiupa, K. S., and Hovorun, D. M. (2018b). Surprising conformers of the biologically important A·T DNA base pairs: QM/QTAIM proofs. *Front. Chem*. 6:8. doi: 10.3389/fchem.2018.00008

Brovarets', O. O., Tsiupa, K. S., and Hovorun, D. M. (2018c). Unexpected A·T(WC)↔A·T(rWC)/A·T(rH) and A·T(H)↔A·T(rH)/A·T(rWC) conformational transitions between the classical A·T DNA base pairs: a QM/QTAIM comprehensive study. *Int. J. Quant. Chem*. 118:e25674. doi: 10.1002/qua.25692

Brovarets', O. O., Tsiupa, K. S., and Hovorun, D. M. (2018e). Novel pathway for mutagenic tautomerization of classical A·T DNA base pairs *via* sequential proton transfer through quasi-orthogonal transition states: a QM/QTAIM investigation. *PLoS ONE*. 13:e0199044. doi: 10.1371/journal.pone.0199044

Brovarets', O. O., Tsiupa, K. S., and Hovorun, D. M. (2018f). The A·T(rWC)/A·T(H)/A·T(rH) ↔ A·T*(rw_{WC})/A·T*(w_H)/A·T*(rw_H) mutagenic tautomerization *via* sequential proton transfer: a QM/QTAIM study. *RSC Adv*. 8, 13433–13445. doi: 10.1039/C8RA01446A

Brovarets', O. O., Voiteshenko, I., Pérez-Sánchez, H. E., and Hovorun, D. M. (2018h). A QM/QTAIM detailed look at the Watson-Crick↔wobble tautomeric transformations of the 2-aminopurine·pyrimidine mispairs. *J. Biomol. Struct. Dynam*. 36, 1649–1665. doi: 10.1080/07391102.2017.1331864

Brovarets', O. O., Voiteshenko, I. S., and Hovorun, D. M. (2018g). Physico-chemical profiles of the wobble↔Watson-Crick G*·2AP(w)↔G·2AP(WC) and A·2AP(w)↔A*·2AP(WC) tautomerisations: A QM/QTAIM comprehensive survey. *Phys. Chem. Chem. Phys*. 20, 623–636. doi: 10.1039/C7CP05139E

Brovarets', O. O., Voiteshenko, I. S., Pérez-Sánchez, H. E., and Hovorun, D. M. (2017). A QM/QTAIM research under the magnifying glass of the DPT tautomerisation of the wobble mispairs involving 2-aminopurine. *New J. Chem*. 41, 7232–7243. doi: 10.1039/C7NJ00717E

Brovarets', O. O., Yurenko, Ye. P., Dubey, I. Y., and Hovorun, D. M. (2012). Can DNA-binding proteins of replisome tautomerize nucleotide bases? *Ab initio* model study. *J. Biomol. Struct. Dynam*. 29, 1101–1109. doi: 10.1080/07391102.2011.672624

Brovarets', O. O., Yurenko, Y. P., and Hovorun, D. M. (2014e). Intermolecular CH···O/N H-bonds in the biologically important pairs of natural nucleobases: a thorough quantum-chemical study. *J. Biomol. Struct. Dynam*. 32, 993–1022. doi: 10.1080/07391102.2013.799439

Brovarets', O. O., Zhurakivsky, R. O., and Hovorun, D. M. (2013a). The physico-chemical "anatomy" of the tautomerisation through the DPT of the biologically important pairs of hypoxanthine with DNA bases: QM and QTAIM perspectives. *J. Mol. Model*. 19, 4119–4137. doi: 10.1007/s00894-012-1720-9

Brovarets', O. O., Zhurakivsky, R. O., and Hovorun, D. M. (2013b). The physico-chemical mechanism of the tautomerisation *via* the DPT of the long Hyp*·Hyp Watson-Crick base pair containing rare tautomer: a QM and QTAIM detailed look. *Chem. Phys. Lett*. 578, 126–132. doi: 10.1016/j.cplett.2013.05.067

Brovarets', O. O., Zhurakivsky, R. O., and Hovorun, D. M. (2014a). Structural, energetic and tautomeric properties of the T·T*/T*·T DNA mismatch involving mutagenic tautomer of thymine: a QM and QTAIM insight. *Chem. Phys. Lett*. 592, 247–255. doi: 10.1016/j.cplett.2013.12.034

Brovarets', O. O., Zhurakivsky, R. O., and Hovorun, D. M. (2014b). Is the DPT tautomerisation of the long A·G Watson-Crick DNA base mispair a source of the adenine and guanine mutagenic tautomers? A QM and QTAIM response to the biologically important question. *J. Comput. Chem*. 35, 451–466. doi: 10.1002/jcc.23515

Brovarets', O. O., Zhurakivsky, R. O., and Hovorun, D. M. (2014c). A QM/QTAIM microstructural analysis of the tautomerisation *via* the DPT of the hypoxanthine·adenine nucleobase pair. *Mol. Phys*. 112, 2005–2016. doi: 10.1080/00268976.2013.877170

Brovarets', O. O., Zhurakivsky, R. O., and Hovorun, D. M. (2014d). Does the tautomeric status of the adenine bases change upon the dissociation of the A*·A_{syn} Topal-Fresco DNA mismatch? A combined QM and QTAIM atomistic insight. *Phys. Chem. Chem. Phys*. 16, 3715–3725. doi: 10.1039/c3cp54708f

Brovarets', O. O., Zhurakivsky, R. O., and Hovorun, D. M. (2015). DPT tautomerisation of the wobble guanine·thymine DNA base mispair is not mutagenic: QM and QTAIM arguments. *J. Biomol. Struct. Dynam*. 33, 674–689. doi: 10.1080/07391102.2014.897259

El-Sayed, A. A., Tamara Molina, A., Alvarez-Ros, M. C., Palafox, M. A. (2015). Conformational analysis of the anti-HIV Nikavir prodrug: comparisons with AZT and thymidine, and establishment of structure-activity relationships/tendencies in other 6′-derivatives. *J. Biomol. Struct. Dynam*. 33, 723–748. doi: 10.1080/07391102.2014.909743

Erdmann, V. A., Markiewicz, W. T., and Barciszewski, J. (2014). *Chemical Biology of Nucleic Acids*. Heidelberg: Springer.

Espinosa, E., Molins, E., and Lecomte, C. (1998). Hydrogen bond strengths revealed by topological analyses of experimentally observed electron densities. *Chem. Phys. Lett*. 285, 170–173. doi: 10.1016/S0009-2614(98)00036-0

Florian, J., Hrouda, V., and Hobza, P. (1994). Proton transfer in the adenine-thymine base pair. *J. Am. Chem. Soc*. 116, 1457–1460. doi: 10.1021/ja00083a034

Frisch, M. J., Head-Gordon, M., and Pople, J. A. (1990). Semi-direct algorithms for the MP2 energy and gradient. *Chem. Phys. Lett*. 166, 281–289. doi: 10.1016/0009-2614(90)80030-H

Frisch, M. J., Trucks, G. W., Schlegel, H. B., Scuseria, G. E., Robb, M. A., Cheeseman, J. R., et al. (2010). *GAUSSIAN 09 (Revision, B.01)*. Wallingford, CT: Gaussian Inc.

Gatti, C., Macetti, G., Boyd, R. J., and Matta, C. F. (2018). An electron density source-function study of DNA base pairs in their neutral and ionized ground states. *J. Comput. Chem*. 39, 1112–1128. doi: 10.1002/jcc.25222

Glushenkov, A. N., and Hovorun, D. M. (2016). Complete set of H-bonded homoassociates of 9-methylguanine by the participation of mutagenic tautomers: quantum-mechanical study. *Repts. Natl. Acad. Sci. Ukraine*. 3, 98–106. doi: 10.15407/dopovidi2016.03.098

Godbeer, A. D., Al-Khalili, J. S., and Stevenson, P. D. (2015). Modelling proton tunnelling in the adenine-thymine base pair. *Phys. Chem. Chem. Phys*. 7, 13034–13044. doi: 10.1039/C5CP00472A

Gorb, L., Podolyan, Y., Dziekonski, P., Sokalski, W. A., and Leszczynski, J. (2004). Double-proton transfer in adenine–thymine and guanine–cytosine base pairs. A post Hartree–Fock *ab initio* study. *J. Am. Chem. Soc.* 126, 10119–10129. doi: 10.1021/ja049155n

Govorun, D. M., Danchuk, V. D., Mishchuk Ya, R, Kondratyuk, I. V., Radomsky, N. F., and Zheltovsky, N. V. (1992). AM1 calculation of the nucleic acid bases structure and vibrational spectra. *J. Mol. Struct*. 267, 99–103. doi: 10.1016/0022-2860(92)87016-O

Govorun, D. M., Kondratyuk, I. V., and Zheltovsky, N. V. (1995a). About physico-chemical mechanisms of hydrogen-tritium exchange of purine nucleotide bases C8H8 groups with water. *Biopol. Cell*. 11, 24–28. doi: 10.7124/bc.0003E9

Govorun, D. M., Kondratyuk, I. V., and Zheltovsky, N. V. (1995b). Prototropic molecular-zwitterion tautomerism of purine. *Biopol. Cell*. 11, 45–50. doi: 10.7124/bc.000402

Gutowski, M., Van Lenthe, J. H., Verbeek, J., Van Duijneveldt, F. B., and Caahalasinski, G. (1986). The basis set superposition error in correlated electronic structure calculations. *Chem. Phys. Lett*. 124, 370–375. doi: 10.1016/0009-2614(86)85036-9

Hariharan, P. C., and Pople, J. A. (1973). The influence of polarization functions on molecular orbital hydrogenation energies. *Theor. Chim. Acta*. 28, 213–222. doi: 10.1007/BF00533485

Hoogsteen, K. (1963). The crystal and molecular structure of a hydrogen-bonded complex between 1-methylthymine and 9-methyladenine. *Acta Cryst*. 16, 907–916. doi: 10.1107/S0365110X63002437

Hovorun, D. M., Gorb, L., and Leszczynski, J. (1999). From the nonplanarity of the amino group to the structural nonrigidity of the molecule: a post-Hartree-Fock *ab initio* study of 2-aminoimidazole. *Int. J. Quantum. Chem.* 75, 245–253. doi: 10.1002/(SICI)1097-461X(1999)75:3<245::AID-QUA14>3.0.CO;2-0

Hratchian, H. P., Schlegel, H. B. (2005). "Finding minima, transition states, and following reaction pathways on *ab initio* potential energy surfaces," in *Theory and applications of computational chemistry: The first 40 years,* eds C. E. Dykstra, G. Frenking, K. S. Kim, and G. Scuseria (*Amsterdam: Elsevier*), 195–249. doi: 10.1016/B978-044451719-7/50053-6

Iogansen, A. V. (1999). Direct proportionality of the hydrogen bonding energy and the intensification of the stretching ν(XH) vibration in infrared spectra. *Spectrochim. Acta Part A* 55, 1585–1612. doi: 10.1016/S1386-1425(98)00348-5

Keith, T. A. (2010). *AIMAll (Version 10.07.01)*. Retrieved from aim.tkgristmill.com.

Kendall, R. A., Dunning Jr, T. H., and Harrison, R. J. (1992). Electron affinities of the first-row atoms revisited. Systematic basis sets and wave functions. *J. Chem. Phys*. 96, 6796–6806. doi: 10.1063/1.462569

Kondratyuk, I. V., Samijlenko, S. P., Kolomiets,' I. M., and Hovorun, D. M. (2000). Prototropic molecular–zwitterionic tautomerism of xanthine and hypoxanthine. *J. Mol. Struct*. 523, 109–118. doi: 10.1016/S0022-2860(99)00385-3

Krishnan, R., Binkley, J. S., Seeger, R., and Pople, J. A. (1980). Self-consistent molecular orbital methods. *XX*. A basis set for correlated wave functions. *J. Chem. Phys*. 72, 650–654. doi: 10.1063/1.438955

Lecomte, C., Espinosa, E., and Matta, C. F. (2015). On atom–atom 'short contact' bonding interactions in crystals. *IUCr J*. 2, 161–163. doi: 10.1107/S2052252515002067

Lee, C., Yang, W., and Parr, R. G. (1988). Development of the Colle-Salvetti correlation-energy formula into a functional of the electron density. *Phys. Rev. B*. 37, 785–789. doi: 10.1103/PhysRevB.37.785

Löwdin, P-O. (1963). Proton tunneling in DNA and its biological implications. *Rev. Mod. Phys*. 35, 724–732. doi: 10.1103/RevModPhys.35.724

Löwdin, P-O. (1966). "Quantum genetics and the aperiodic solid: some aspects on the biological problems of heredity, mutations, aging, and tumors in view of the quantum theory of the DNA molecule," in *Advances in Quantum Chemistry*, : ed P.-O. Löwdin (New York, NY; London: Academic Press), 213–360. doi: 10.1016/S0065-3276(08)60076-3

Mata, I., Alkorta, I., Espinosa, E., and Molins, E. (2011). Relationships between interaction energy, intermolecular distance and electron density properties in hydrogen bonded complexes under external electric fields. *Chem. Phys. Lett*. 507, 185–189. doi: 10.1016/j.cplett.2011.03.055

Matta, C. F. (2010). How dependent are molecular and atomic properties on the electronic structure method? Comparison of Hartree-Fock, DFT, and MP2 on a biologically relevant set of molecules. *J. Comput. Chem.* 31, 1297–1311. doi: 10.1002/jcc.21417

Matta, C. F. (2014). Modeling biophysical and biological properties from the characteristics of the molecular electron density, electron localization and delocalization matrices, and the electrostatic potential. *J. Comput. Chem*. 35, 1165–1198. doi: 10.1002/jcc.23608

Matta, C. F., Castillo, N., and Boyd, R. J. (2006a). Atomic contributions to bond dissociation energies in aliphatic hydrocarbons. *J. Chem. Phys*. 125;204103. doi: 10.1063/1.2378720

Matta, C. F., Castillo, N., and Boyd, R. J. (2006b). Extended weak bonding interactions in DNA: π-stacking (base-base), base-backbone, and backbone-backbone interactions. *J. Phys. Chem. B* 110, 563–578. doi: 10.1021/jp054986g

Matta, C. F., and Hernández-Trujillo, J. (2003). Bonding in polycyclic aromatic hydrocarbons in terms of the electron density and of electron delocalization. *J. Phys. Chem.* 107, 7496–7504. doi: 10.1021/jp034952d

McFadden, J., and Al-Khalili, J. (2018). The origins of quantum biology. *Proc. R Soc.* 474:20180674. doi: 10.1098/rspa.2018.0674

Meisner, J., and Kastner, J. (2016). Atom tunnelling in chemistry. *Angew. Chem. Int/ Ed*. 55, 5400–5413. doi: 10.1002/anie.201511028

Nikolaienko, T. Y., Bulavin, L. A., and Hovorun, D. M. (2011). How flexible are DNA constituents? The quantum-mechanical study. *J. Biomol. Struct. Dynam*. 29, 563–575. doi: 10.1080/07391102.2011.10507406

Nikolaienko, T. Y., Bulavin, L. A., and Hovorun, D. M. (2012). Bridging QTAIM with vibrational spectroscopy: the energy of intramolecular hydrogen bonds in DNA-related biomolecules. *Phys. Chem. Chem. Phys*. 14, 7441–7447. doi: 10.1039/c2cp40176b

Nikolova, E. N., Zhou, H., Gottardo, F. L., Alvey, H. S., Kimsey, I. J., and Al-Hashimi, H. M. (2014). A historical account of Hoogsteen base pairs in duplex DNA. *Biopolymers* 99, 955–968. doi: 10.1002/bip.22334

Palafox, M. A. (2014). Molecular structure differences between the antiviral nucleoside analogue 5-iodo-2'-deoxyuridine and the natural nucleoside 2'-deoxythymidine using MP2 and DFT methods: conformational analysis, crystal simulations, DNA pairs and possible behavior. *J. Biomol. Struct. Dynam*. 32, 831–851. doi: 10.1080/07391102.2013.789402

Parker, B. R., and Van Everv, J. (1971). Quantum tunnelling in DNA. *Chem. Phys. Lett*. 8, 94–99. doi: 10.1016/0009-2614(71)80586-9

Parr, R. G., and Yang, W. (1989). *Density-Functional Theory of Atoms and Molecules*. Oxford: Oxford University Press.

Peng, C., Ayala, P. Y., Schlegel, H. B., and Frisch, M. J. (1996). Using redundant internal coordinates to optimize equilibrium geometries and transition states. *J. Comput. Chem.* 17, 49–56. doi: 10.1002/(SICI)1096-987X(19960115)17:1<49::AID-JCC5>3.0.CO;2-0

Poltev, V. I., Anisimov, V. M., Sanchez, C., Deriabina, A., Gonzalez, E., Garcia, D., et al. (2016). Analysis of the conformational features of Watson–Crick duplex fragments by molecular mechanics and quantum mechanics methods. *Biophysics* 61, 217–226. doi: 10.1134/S0006350916020160

Pous, J., Urpi, L., Subirana, J. A., Gouyette, C., Navaza, J., and Campos, J. L. (2008). Stabilization by extra-helical thymines of a DNA duplex with Hoogsteen base pairs. *J. Am. Chem. Soc*. 130, 6755–6760. doi: 10.1021/ja078022+

Pusuluk, O., Torun, G., and Deliduman, C. (2018). Quantum entanglement shared in hydrogen bonds and its usage as a resource in molecular recognition. *Mod. Phys. Lett*. 32:1850308. doi: 10.1142/S0217984918503086

Roßbach, S., and Ochsenfeld, Ch. (2017). Influence of coupling and embedding schemes on QM size convergence in QM/MM approaches for the example of a proton transfer in DNA. *J. Chem. Theor. Comput*. 13, 1102–1107. doi: 10.1021/acs.jctc.6b00727

Saenger, W. (1984). *Principles of Nucleic Acid Structure. New York*, NY: *Springer*.

Shekaari, A., and Jafari, M. (2019). Modeling the action of environment on proton tunneling in the adenine–thymine base pair. *Prog. Biophys. Mol. Biol*. doi: 10.1016/j.pbiomolbio.2019.07.002. [Epub ahead of print].

Sinden, R. R. (1994). *DNA Structure and Function*. London: Academic Press.

Smedarchina, Z., Siebrand, W., and Fernández-Ramos, A. (2018). Entanglement and co-tunneling of two equivalent protons in hydrogen bond pairs. *J. Chem. Phys.* 148, 102307–1–102307-15. doi: 10.1063/1.5000681

Sordo, J. A. (2001). On the use of the Boys–Bernardi function counterpoise procedure to correct barrier heights for basis set superposition error. *J. Mol. Struct*. 537, 245–251. doi: 10.1016/S0166-1280(00)00681-3

Sordo, J. A., Chin, S., and Sordo, T. L. (1988). On the counterpoise correction for the basis set superposition error in large systems. *Theor. Chim. Acta*. 74, 101–110. doi: 10.1007/BF00528320

Sponer, J., and Lankas, F. (2006). *Computational Studies of RNA and DNA*. Springer: *Netherlands*.

Srivastava, R. (2019). The role of proton transfer on mutations. *Front Chem*. 7:536. doi: 10.3389/fchem.2019.00536

Szabat, M., and Kierzek, R. (2017). Parallel-stranded DNA and RNA duplexes: structural features and potential applications. *FEBS J*. 284, 3986–3998. doi: 10.1111/febs.14187

Tirado-Rives, J., and Jorgensen, W. L. (2008). Performance of B3LYP density functional methods for a large set of organic molecules. *J. Chem. Theory Comput*. 4, 297–306. doi: 10.1021/ct700248k

Turaeva, N., and Brown-Kennerly, V. (2015). Marcus model of spontaneous point mutation in DNA. *Chem. Phys*. 461, 106–110. doi: 10.1016/j.chemphys.2015.09.005

Watson, J. D., and Crick, F. H. C. (1953a). The structure of DNA. *Cold Spring Harb. Symp. Quant. Biol*. 18, 123–131. doi: 10.1101/SQB.1953.018.01.020

Watson, J. D., and Crick, F. H. C. (1953b). Molecular structure of nucleic acids: a structure for deoxyribose nucleic acid. *Nature*. 171, 737–738. doi: 10.1038/171737a0

Wigner, E. (1932). Über das Überschreiten von Potentialschwellen bei chemischen Reaktionen [Crossing of potential thresholds in chemical reactions]. *Zeits Physik Chem*. 19, 203–216. doi: 10.1515/zpch-1932-1920

Ye, M. Y., Zhu, R. T., Li, X., Zhou, X. S., Yin, Z. Z., Li, Q., et al. (2017). Adaptively recognizing parallel-stranded duplex structure for fluorescent DNA polarity analysis. *Anal. Chem*. 89, 8604–8608. doi: 10.1021/acs.analchem.7b02467

Zhou, H. (2016). *Occurrence and Function of Hoogsteen Base Pairs in Nucleic Acids*. PhD Thesis, Duke University. Available online at: https://dukespace.lib.duke.edu/dspace/handle/10161/12892

Conflict of Interest Statement: The authors declare that the research was conducted in the absence of any commercial or financial relationships that could be construed as a potential conflict of interest.